Resource

Cell

Portable, On-Demand Biomolecular Manufacturing

Graphical Abstract

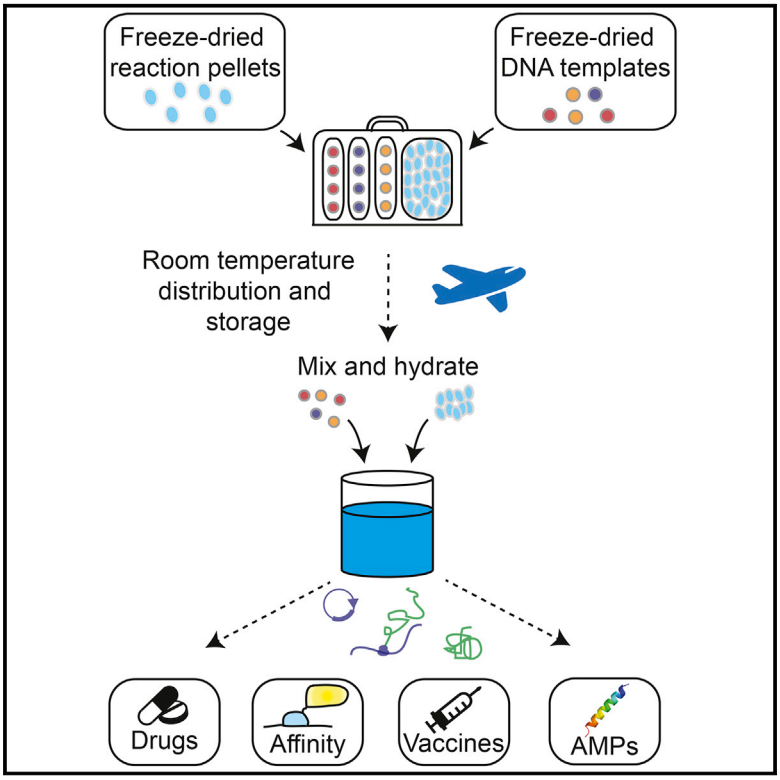

Authors

Keith Pardee, Shimyn Slomovic, Peter Q. Nguyen, ..., Christopher N. Boddy, Neel S. Joshi, James J. Collins

Correspondence

jimjc@mit.edu

In Brief

Ready-to-use preparations enable on-site, on-demand production of biomolecules like antimicrobials and vaccines without refrigeration or specialized equipment.

Highlights

- A cell-free platform for on-site, on-demand biomolecular manufacturing
- Distribution and production of therapeutics and biomolecules without a cold chain
- Synthesis and functional validation of antimicrobial peptides and vaccines
- Combinatorial manufacturing of antibody mimetic conjugates and small molecules

Data Resources

KX461959
KX461960
KX461961
KX461962
KX461963

Pardee et al., 2016, Cell *167*, 248–259
September 22, 2016
http://dx.doi.org/10.1016/j.cell.2016.09.013

CellPress

Cell

Resource

Portable, On-Demand Biomolecular Manufacturing

Keith Pardee,[1,10] Shimyn Slomovic,[2,10] Peter Q. Nguyen,[3,10] Jeong Wook Lee,[2,3,10] Nina Donghia,[3] Devin Burrill,[3] Tom Ferrante,[3] Fern R. McSorley,[4] Yoshikazu Furuta,[2] Andyna Vernet,[3] Michael Lewandowski,[3] Christopher N. Boddy,[4] Neel S. Joshi,[3,5] and James J. Collins[2,3,6,7,8,9,11,*]

[1]Leslie Dan Faculty of Pharmacy, University of Toronto, Toronto, ON M5S 3M2, Canada
[2]Institute for Medical Engineering and Science, Massachusetts Institute of Technology, Cambridge, MA 02139, USA
[3]Wyss Institute for Biologically Inspired Engineering, Harvard University, Boston, MA 02115, USA
[4]Department of Chemistry and Biomolecular Sciences, University of Ottawa, Ottawa, ON K1N 6N5, Canada
[5]School of Engineering and Applied Sciences, Harvard University, Cambridge, MA 02138, USA
[6]Department of Biological Engineering, Massachusetts Institute of Technology, Cambridge, MA 02139, USA
[7]Synthetic Biology Center, Massachusetts Institute of Technology, Cambridge, MA 02139, USA
[8]Harvard-MIT Program in Health Sciences and Technology, Cambridge, MA 02139, USA
[9]Broad Institute of MIT and Harvard, Cambridge, MA 02142, USA
[10]Co-first authors
[11]Lead contact
*Correspondence: jimjc@mit.edu
http://dx.doi.org/10.1016/j.cell.2016.09.013

SUMMARY

Synthetic biology uses living cells as molecular foundries for the biosynthesis of drugs, therapeutic proteins, and other commodities. However, the need for specialized equipment and refrigeration for production and distribution poses a challenge for the delivery of these technologies to the field and to low-resource areas. Here, we present a portable platform that provides the means for on-site, on-demand manufacturing of therapeutics and biomolecules. This flexible system is based on reaction pellets composed of freeze-dried, cell-free transcription and translation machinery, which can be easily hydrated and utilized for biosynthesis through the addition of DNA encoding the desired output. We demonstrate this approach with the manufacture and functional validation of antimicrobial peptides and vaccines and present combinatorial methods for the production of antibody conjugates and small molecules. This synthetic biology platform resolves important practical limitations in the production and distribution of therapeutics and molecular tools, both to the developed and developing world.

INTRODUCTION

Synthetic biology applies rational design principles of engineering to molecular biology to build genetic devices, which have begun to impact the diagnostic and therapeutic space. This approach has helped to create whole-cell biosensors (Kobayashi et al., 2004), genetically modified probiotics (Danino et al., 2015), and a growing capability for cell-based biomolecular manufacturing. Rooted in genetically engineered production cell lines, biosynthesis is increasingly a mainstay for industrial drug production (Fossati et al., 2014), protein therapeutics (Dimitrov, 2012), fuels (Torella et al., 2015), and other commodities (Chubukov et al., 2016). However, the reliance on living cellular hosts to operate the genetic programs that underpin biosynthesis is accompanied by biosafety regulations, practical hurdles, and specialized skills that limit their operation to laboratory settings. Therefore, vaccines and other protein-based biomolecules must be globally distributed from centralized foundries and, most often, require a cold chain for stability. These limitations impact distribution costs and highlight the challenge of delivering the benefits of these technologies to developing regions. We recently reported a method for the safe deployment of genetically encoded tools (Pardee et al., 2014). Using freeze-dried, cell-free (FD-CF) expression machinery on paper, we generated a platform that retains the fundamental protein synthesis capability of live cells while remaining abiotic, sterile, and portable. In combination with toehold switch RNA sensors (Green et al., 2014), this platform was used to demonstrate a new class of low-cost diagnostic tools (Pardee et al., 2016).

FD-CF reactions offer additional venues for the distributed use of synthetic biology apart from diagnostics, such as the exciting prospect of the portable manufacture of pharmaceuticals, therapeutic proteins, and other biomolecules. In recent years, in vitro biosynthesis from fresh or frozen lysates has developed remarkably, including the biomanufacture of difficult molecules that cause cell toxicity and the incorporation of non-canonical elements (Amiram et al., 2015; Dudley et al., 2015; Karim and Jewett, 2016; Sullivan et al., 2016; Welsh et al., 2012; Zawada et al., 2011). These advances have thus far been tied to laboratory settings where the necessary skills and equipment are found. Building off of this foundation, the proposed use of FD-CF systems, with their long-term activity at room temperature (>1 year) and ease of operation, could alleviate both the restrictions of live-cell biosynthesis and cold-chain distribution requirements (Pardee et al., 2014). Recent reports draw emphasis to a pressing need for the decentralization of therapeutic biomanufacturing, offering novel alternatives that, nonetheless, require expensive, large equipment and highly skilled operators or yet rely on production from living cells (Adamo et al., 2016; Perez-Pinera

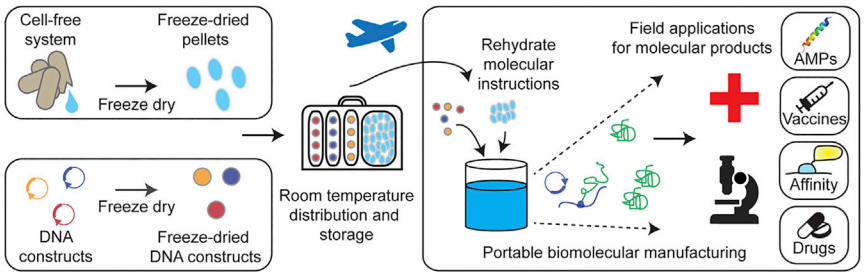

Figure 1. Portable Biomolecular Manufacturing

By pairing freeze-dried, cell-free reaction pellets with lyophilized DNA encoding the instructions for protein synthesis, therapeutics and other molecular tools can be manufactured on site, on demand through the simple addition of water, avoiding the normally required cold-chain distribution. Here, we demonstrate the use of this portable biomanufacturing platform for the production of a diverse range of functionally active products, including AMPs, vaccines, affinity conjugates, and small molecules.

et al., 2016). Previous work has demonstrated protein production from lyophilized reactions, which strongly supports the notion of advancing this concept further toward on-demand, local biomanufacturing (Salehi et al., 2016; Smith et al., 2014). In addition to portability, the FD-CF format has all of the advantages that are innate to in vitro biosynthesis. Moreover, with buffers, cellular machinery, and molecular instructions all compressed into a single FD reaction pellet, on-demand, on-site activation would only require the addition of water and yields product within 1–2 hr, without the need for specialized equipment and skill. This system could be applied for global health and personalized medicine, making scalable molecular synthesis available to anyone with FD reagents and DNA-encoding biosynthesis instructions.

Here, we present a series of vignettes describing the production of a diverse set of therapeutics and molecular tools for clinical and research environments using FD-CF reaction pellets (Figure 1). Nested within this proof of concept is a drive to create inexpensive alternatives for developing world applications where cost is a major factor to access. We begin with the production of two therapeutic classes of molecules: antimicrobial peptides (AMPs) and vaccines. For the former, we demonstrate purification schemes and validate antimicrobial activity. For the latter, we verify the expression of three vaccine antigens, including the scaled-up production and functional characterization of the diphtheria toxoid antigen (DT), which is administered to an animal model to confirm a successful immune response. Next, we establish a novel combinatorial approach to generate 90 possible affinity conjugates for applications in research and healthcare, of which a subset are functionally validated. Finally, we reconstitute a multi-enzyme biosynthesis pathway for small-molecular therapeutic production and offer a mix-and-match method to synthesize multiple pathway products, which are confirmed using mass spectrometry (MS).

RESULTS

Antimicrobial Peptides

AMPs are a diverse peptide class that evolved as defense molecules against infection by interfering with protective cell layers and intracellular components. Given their wide target range (bacteria, viruses, fungi, and cancer) (Gaspar et al., 2013), compact molecular structure (<10 kDa), and reports of their expression using non-lyophilized lysates (Lee et al., 2010; Martemyanov et al., 2001), we sought to express and functionally validate these promising alternatives to classic antibiotics using the FD-CF format. DNA templates encoding ten different AMPs (B1CTcu1, PEP3, CA(1-7)M(2-9), BP100, Magainin 2, Cecropin P1, Cecropin B, Bac7(1-35), Tachystatin A1, and Opistoporin 1) were added to a recombinant CF reaction mixture and lyophilized (Table S1). Following subsequent rehydration and incubation, electrophoresis and staining confirmed that all AMPs were produced (Figure 2A). To support applications in which background proteins might interfere, we also designed versions of three AMPs to contain a leader sequence for increased stability, an affinity tag for purification, and a Factor Xa protease site for subsequent removal of these added residues, which could dampen bioactivity. His_6- and FLAG-tagged variants of each AMP were successfully synthesized and were confirmed by western blot (WB) (Figure 2B).

Lyophilized, bacterial lysates prepared "in house" could serve as vastly more economical alternatives to commercial lysate-based kits or recombinant kits. Therefore, the expression of FLAG-tagged Cecropin P1 using lyophilized, in-house lysate was benchmarked against a S30 T7 lysate-based kit (Promega; L1110) and a recombinant system (NEB; E6800L). A semiquantitative WB confirmed successful AMP production from in-house lysate, which outperformed the S30 T7 kit and yielded 20%–40% of the amount produced with the recombinant system (Figure S1A). Next, affinity purification and Factor Xa cleavage were demonstrated, resulting in the release of a peptide product of expected size (Figure 2C). Cleavage was alternatively performed in a crude AMP reaction (Figure S1B).

The small AMP size offers an alternative, simple purification route based on molecular weight filtration (Figure 2D). Accordingly, AMP synthesis reactions were passed through a 10 kDa filter, which resulted in the retention of CF machinery while allowing passage and recovery of the AMPs (Figure 2D). Using custom-synthesized AMP standards (LifeTein), semiquantitative analysis was applied to a subset of weight-filtered AMP reactions for Cecropin P1, Cecropin B, CA(1-7)M(2-9), and BP100. Yields of soluble peptide were approximated at 125–156 ng/μL, 188–219 ng/μL, 94–125 ng/μL, and 63–94 ng/μL, respectively (Figure S1C). Finally, AMP bioactivity was tested and exhibited a growth inhibition effect on either *E. coli* (Gram-negative) or *B. subtilis* (Gram-positive) (Figures 2E and 2F, respectively, and Figures S1D and S1E, respectively). Importantly, isolation of the AMPs from the CF machinery was not required for bioactivity, highlighting an added flexibility that suggests that, in appropriate cases, such as for topical

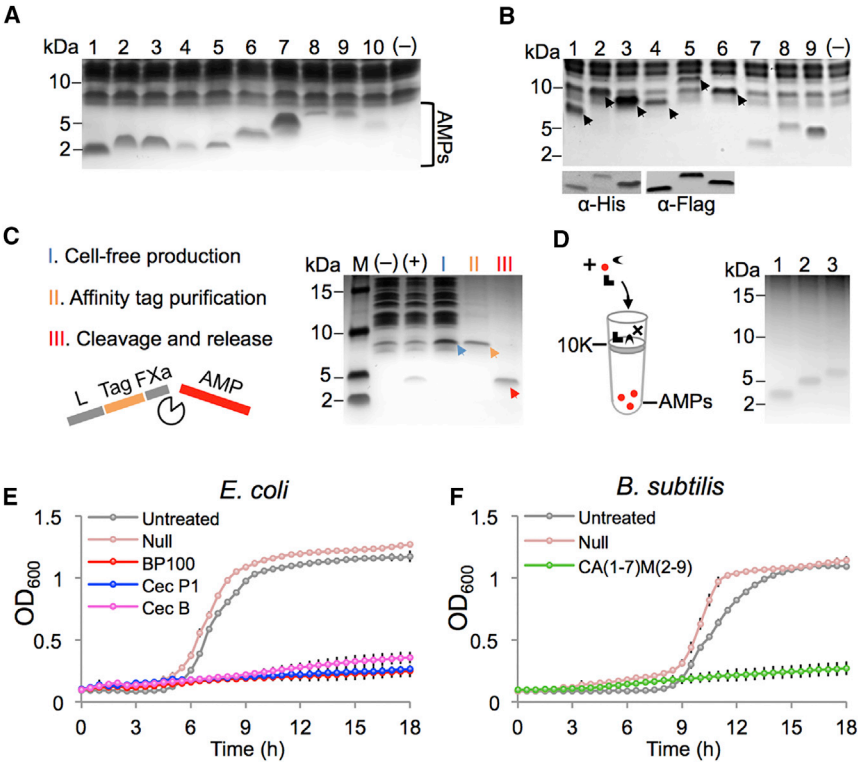

Figure 2. FD-CF Production of AMPs

(A) Coomassie gel of 10 AMPs (L to R): B1CTcu1, PEP3, CA(1-7)M(2-9), BP100, Magainin 2, Cecropin P1, Cecropin B, Bac7(1-35), Tachystatin A1, Opistoporin 1. (–) indicates null reaction lacking DNA template. A bracket frames the molecular weight range of AMPs, while bands above the bracket originate from CF machinery.

(B) Coomassie gel of three peptides (L to R), Magainin 2, Opistoporin 1, and Cecropin P1, that were designed to contain (from N to C terminus) a leader sequence (L), affinity tag (His_{x6} or FLAG), Factor Xa cleavage site, and AMP sequence, allowing purification as described in (C). Lanes 1–3, His-tagged; lanes 4–6, FLAG-tagged; lanes 7–9, non-tagged versions. Arrows indicate relevant bands in lanes 1–6. Below lanes 1–3 and lanes 4–6 are WBs of the triplets with His or FLAG probes, respectively.

(C) Left: peptide purification scheme. Right: Coomassie gel demonstrating FLAG-based purification and cleavage for Cecropin P1. M, molecular weight ladder; (–), null reaction; (+), non-tagged Cecropin P1 size control; I, FLAG-tagged Cecropin P1 size control (blue arrow); II, purified FLAG-tagged Cecropin P1 (orange arrow); III, Factor Xa cleavage and release of the purified AMP (red arrow).

(D) Left: molecular weight filtration scheme of non-tagged AMPs (red circles). Transcription and translation machinery (black icon mix) retained on 10 kDa membrane, while non-tagged AMPs (red circle) pass through. Right: Coomassie gel of three example AMPs (L to R): Magainin 2, Cecropin P1, and Cecropin B.

(E) Chart showing growth inhibition assay of *E. coli* subjected to three individual AMPs (indicated in the chart legend) alongside untreated and null samples. OD_{600} was measured every 30 min for 18 hr.

(F) Chart showing growth inhibition assay of *B. subtilis* subjected to one AMP, as described above.

All data points in (E) and (F) represent the mean ± SD of three biological replicates.

administration, AMPs could be rapidly synthesized and applied effectively in crude format.

Portable Vaccine Production

Vaccines are one of the most powerful tools in disease prevention, with childhood diseases, such as polio, smallpox, and diphtheria, largely contained owing to systematic immunizations. However, distribution to the developing world is challenging, primarily due to costs and cold-chain requirements. While some vaccines can be lyophilized, temperature-controlled distribution cannot be avoided for others. Citing previous reports of the in vitro expression of vaccine antigens (Palmenberg, 1982; Welsh et al., 2012; Zichel et al., 2010), we sought to explore whether biosynthesis could be performed on site using FD-CF reactions, rather than restricted to a centralized production facility (Figure 3A). We began with the expression of vaccine antigens for botulinum (neurotoxin fragment, HcE) (Zichel et al., 2010), anthrax (protective antigen, PA), and diphtheria (Diphtheria toxoid, DT), which resulted in clear bands of the expected molecular weights (Figure 3B). Diphtheria infections can lead to severe symptoms, including death. It remains endemic in developing countries that represent 80%–90% of global cases (Dandinarasaiah et al., 2013). The DT antigen was chosen for further characterization, as it is sensitive to both heat and freezing, designating it as an especially challenging vaccine for global distribution (WHO, 2014a).

Fresh, recombinant CF reagents were used to test the expression levels of different DT toxoid antigens (Collier, 2006; Giannini et al., 1984; Gupta et al., 1997). Among those tested, the 51E/148K variant (DT5) and 52E variant (DT6), both containing an N-terminal leader and FLAG-tag, displayed the highest expression levels (Figure S2A and Table S1). Next, the DT5 and DT6 antigens were successfully produced using lyophilized, recombinant reagents, and yield was measured via quantitative fluorescent western blotting (QFWB), which revealed 768 ng/μL (DT5) and 1341 ng/μL (DT6) of soluble protein (Figures S2B and S2C). Correct protein folding, critical for the induction of antibody (Ab)-based immunity, was evaluated via an enzyme-linked immunosorbent assay (ELISA). Both antigens successfully bound to commercial anti-DT Abs, indicating correct protein conformation (Figure 3C). Similar to AMP expression using lyophilized lysates prepared in house, we tested whether DT5 could be produced from this inexpensive source. First, multiple combinations of Mg-glutamate (Mg-Glu) and K-glutamate (K-Glu) concentrations were applied to fresh, in-house lysate to determine optimal expression conditions for DT5, showing 6 mM Mg-Glu + 110 mM K-Glu as ideal concentrations (Figure S2D). DT5 was then produced from FD, in-house lysate under these conditions and was compared to a sample produced from a lyophilized, commercial S30 T7 lysate, resulting in comparable expression levels (Figure S2E).

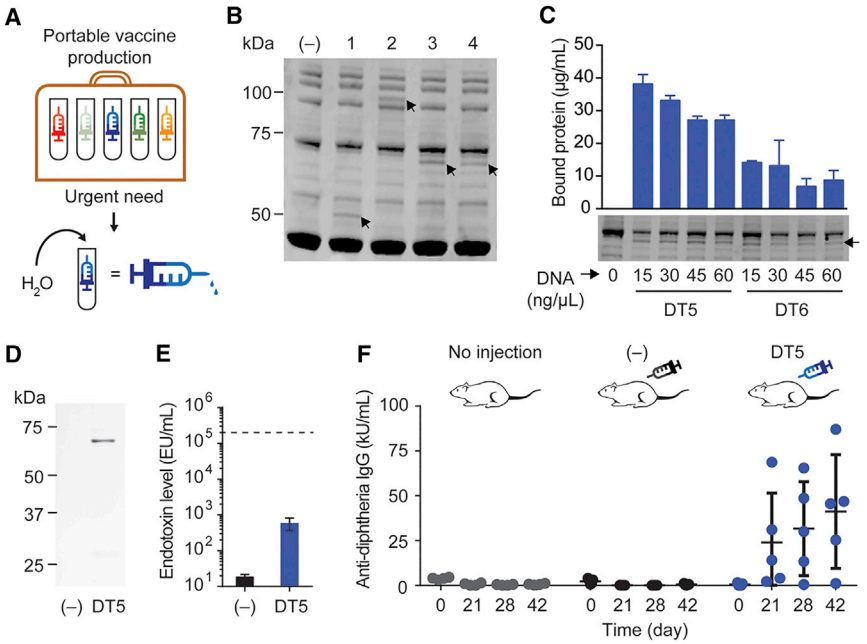

Figure 3. Toward Portable Vaccine Production

(A) Schematic illustrating the distribution of FD-CF reactions for on-demand vaccine biomanufacturing.

(B) Coomassie gel displaying FD-CF reactions producing (L to R): HcE (50 kDa), PA (100 kDa), DT5 (63 kDa), or DT6 (63 kDa). (–) indicates a negative control lacking DNA. Arrows indicate product bands.

(C) Below, Coomassie gel showing DT5 and DT6 generated with increasing amounts of DNA input, as indicated. An arrow indicates predicted product size. Above, ELISA measuring binding capability using plates coated with anti-DT antibody. Data represent the mean ± SD of three replicates.

(D) Coomassie gel showing DT5 antigen (100 μg/mL) prepared via anti-FLAG purification and buffer exchange. (–) indicates a DNA null reaction that underwent identical expression and purification steps.

(E) Limulus amebocyte lysate (LAL) assay measuring endotoxin level of the purified DT5 vaccine. (–) indicates the same DNA null reaction used in (D). Data represent the mean ± SD of three replicates. Dashed line indicates the recommended guideline for DT vaccines.

(F) ELISA analysis measuring the immune response (anti-diphtheria IgG Abs) using plates coated with commercial DT antigen. Blood was drawn on days 0 (before injection), 21, 28, and 42 to test for the induction of Ab production. (–) indicates a group of mice injected with the same DNA null reaction used in (D). Data show the average and ± SD of each group with individual data points (habitat control, n = 4; DNA null control, n = 5; DT5 vaccine, n = 5).

To test methods that might increase DT5 levels, FD-CF reactions were supplemented with a disulfide bond enhancer (DSE), which resulted in a marked increase in band intensity (Figure S2F). The addition of DSE, which can be generated in house or purchased, improves yield by ensuring proper disulfide bridge formation (Goerke and Swartz, 2008). Toward a similar agenda, DT6 levels were assessed after applying a dialysis membrane to the hydrated reaction, providing the CF expression machinery access to a reservoir of molecular reagents while restricting the components to the original, small volume (Noireaux and Libchaber, 2004; Spirin et al., 1988). This approach also led to increased yield when compared to a non-dialyzed reaction (Figure S2G).

The final stage focused on confirming the induction of anti-DT IgG Ab expression in an animal model. First, DT5 was produced from a FD-CF reaction pellet (originating from 900 μl of recombinant, CF reagent) and was isolated via its FLAG tag (Figures 3D and S2H). Next, endotoxin levels were evaluated using the industry standard limulus amebocyte lysate (LAL) assay and showed an extremely low level of endotoxin (596 EU/mL), referencing guidelines for toxoid-based vaccines (<200,000 EU/mL) (Figure 3E) (Brito and Singh, 2011). DT5 was injected into mice (2.5 μg per mouse per injection) at three time points (days 0, 7, and 14), and blood was drawn (days 0, 21, 28, and 42) to test for Ab production. Accompanying the test group were two control groups: non-injected mice and mice injected with the products of a DNA null control (consisting of a FD-CF reaction lacking DT5-encoding plasmid, which underwent identical expression, purification, and injection steps compared to the DT5 test sample). No mice exhibited signs of ill effect from injections throughout the experiment. Crucially, a strong induction of anti-DT IgG Ab production in DT5-treated mice was detected beginning at 3 weeks after the first injection (quantified via ELISA), and no induction was observed in either control group (Figure 3F).

On-Demand Production of Combinatorial Antibody Analogs

Ab-based tools, such as ELISA, fluorescence-activated cell sorting (FACS), and immunofluorescence imaging, have long been used as target-specific reagents in research and clinical applications. Abs have recently begun to revolutionize therapeutics by enabling targeted treatment of diseases, including cancer (Scott et al., 2012), immune disorders (Wang et al., 2015), viral (Ng et al., 2010), and bacterial infections (Kontermann, 2012), as well as targeted delivery of antibiotics (Lehar et al., 2015). Abs have been expressed using laboratory-based CF systems; however, their structural complexity, disulphide bonds, and post-translational modification requirements make their production challenging (Patel et al., 2011; Ryabova et al., 1997). Directed evolution and other engineering techniques have expanded the repertoire of such tools, creating designer affinity molecules, including DARPins and Nanobodies, which are artificial ankyrin repeat proteins and single-chain camelid immunoglobulin fragments, respectively (Desmyter et al., 2015; Plückthun, 2015). Such designer affinity molecules are under development as potential therapeutics, such as Abicipar (anti-VEGF DARPin) and Ozoralizumab (anti-TNFα Nanobody). While Abs and their analogs are powerful tools, their high production cost and need for cold storage limit their distribution and utility. Accordingly, we focused on the FD-CF biosynthesis of DARPin- and Nanobody-based affinity molecules (Doshi et al., 2014; Plückthun, 2015).

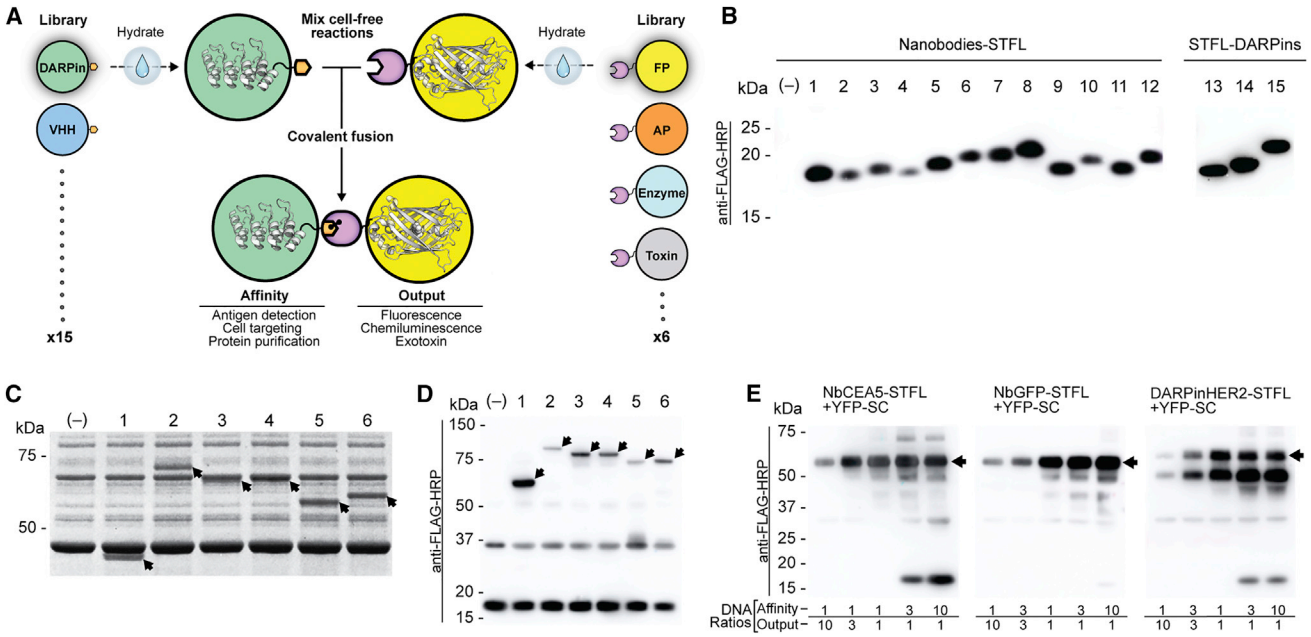

Figure 4. FD-CF Production of On-Demand Affinity Products

(A) Affinity components are composed of binding domains: single-domain VHH Abs (Nanobodies) or Ab mimetics (DARPins) genetically fused to a SpyTag (ST) peptide. Output components are functional domains genetically fused to a SpyCatcher (SC) domain. Mixing the desired affinity and output components expressed in FD-CF reactions results in covalent fusion via the SpyTag-SpyCatcher interaction.

(B) Anti-FLAG WB showing FD-CF expression of 12 Nanobodies and three DARPins containing ST-FLAG tags (STFL). Specific antigen targets are: (1) CEA5, (2) dengue Virus NS1, (3) GFP, (4) HIV p23-gag, (5) norovirus capsid VP1, (6) rotavirus capsid VP6, (7) *C. difficile* exotoxin TcdA, (8) *P. falciparum* VAR2CSA, (9) GLUT1, (10) mCherry, (11) Vimentin, (12) Glycophorin A, (13) HER-2, (14) VEGF-A, and (15) epCAM. (–) indicates a DNA null control reaction.

(C) Coomassie gel showing expression of six different output domains, including fluorescent proteins (YFP, lane 1), enzymes (α-amylase, PhoAP, and SanaAP, lanes 2–4), and cellular toxins (*P. aeruginosa* and *C. diptheriae* exotoxins, lanes 5 and 6), all expressed as SC fusions. Arrows indicate relevant protein bands. (–) indicates a DNA null control.

(D) Anti-FLAG WB showing covalently linked proteins (indicated by arrows) produced by mixing Nanobody anti-CEA5-STFL reactions with output component reactions. Lanes: (–), DNA null; 1, YFP-SC; 2, ∝-amylase-SC; 3, PhoAP-SC; 4, SanaAP-SC; 5, *P. aeruginosa* exotoxin-SC; 6, *C. diptheriae* exotoxin-SC.

(E) Anti-FLAG WB showing one-pot manufacturing of affinity-output proteins, produced by mixing DNA templates encoding different affinity components (left, anti-CEA5-STFL Nanobody; middle, anti-GFP-STFL Nanobody; right, STFL-anti-HER2 DARPin) with DNA encoding the YFP-SC output component in a single FD-CF reaction. Template ratios are shown below.

We designed templates encoding DARPins and Nanobodies specific to 15 diverse molecular targets: fluorophores (GFP, mCherry), cancer-specific epitopes (CEA5, GLUT-1, HER2, epCAM), a cell marker (Vimentin), a cytokine (VEGF-A), a cell-specific epitope (glycophorin A), parasite antigens (VAR2CSA), virus epitopes (dengue, HIV, norovirus, rotavirus), and a *C. difficile* exotoxin (TcdA) (Table S1). Each sequence was appended with a ''SpyTag'' and FLAG-tag. Engineered as a split protein from the *Streptococcus pyogenes* fibronectin-binding protein, the SpyTag forms a spontaneous covalent bond with the ''SpyCatcher'' protein fragment (Zakeri et al., 2012). Here, a sequence encoding the SpyCatcher was added to a series of output domains: yellow fluorescent protein (YFP), α-amylase, *E. coli* alkaline-phosphatase (PhoAP), *S. ana-3* alkaline-phosphatase (SanaAP), *P. aeruginosa* exotoxin, and *C. diptheriae* exotoxin. By incorporating the SpyTag-SpyCatcher scheme into a modular series of affinity proteins and output domains expressed separately, we envisioned a means to generate user-defined de novo protein fusions (Figure 4A). This portable, combinatorial toolbox would allow end users to link a Nanobody or DARPin of choice to a desired output function, such as fluorescence, enzymatic activity, or targeted toxicity, with potentially 90 unique combinations. Anti-FLAG WBs verified the expression of all 15 affinity proteins in FD-CF reactions (Figure 4B). To calibrate Nanobody production using FD-CF, recombinant material, we tested the expression levels of soluble NbTcdA and NbCEA5 using QFWB and measured a yield of 66.4 μg/mL and 280 μg/mL, respectively (Figures S2B and S2C). The FD-CF biosynthesis of all SpyCatcher functional domains was confirmed via Coomassie staining (Figure 4C). To test the option of post-translationally mixing affinity- and output products to create de novo fusions, the anti-CEA5 Nanobody was combined with each of the output products, resulting in six different conjugates (Figure 4D). YFP-SpyCatcher was likewise combined with all 15 different SpyTag affinity domains (Figure S3A). Also, pre-translational single-pot reactions were performed, in which the DNA templates encoding three different Spytagged affinity proteins were each titrated with the YFP-SpyCatcher DNA template to test whether the proteins could be co-expressed and spontaneously pair, as well as to establish an optimal template input ratio to produce the final fusion products (Figure 4E).

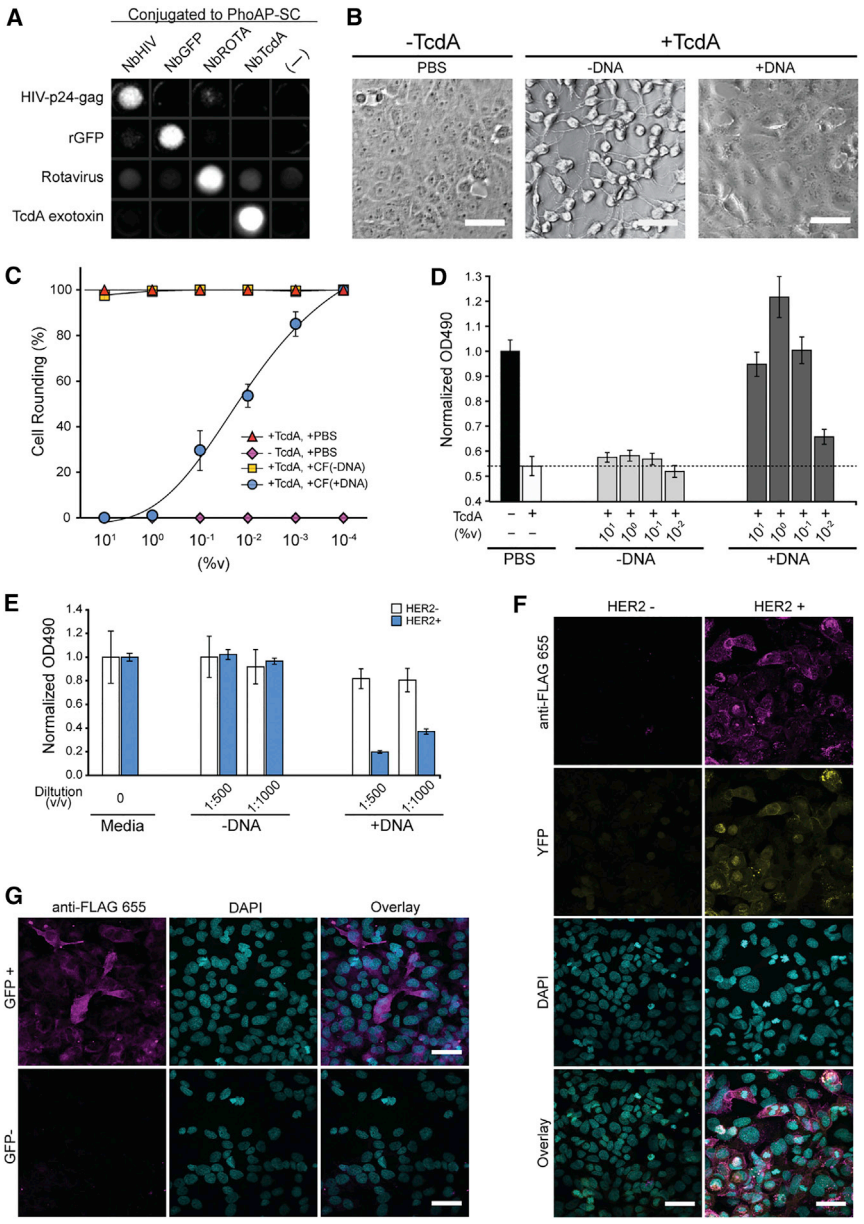

Figure 5. Functional Activity of On-Demand Affinity Products

(A) Chemiluminescent dot blot showing binding of affinity-AP conjugates fused to *E. coli* alkaline phosphatase (PhoAP-SC) to their antigens, listed at left. All rows were normalized for signal intensity across blots. (–) indicates a control in which PhoAP-SC lacking an affinity component was used.

(B) Phase contrast microscopy of Vero cells exposed to: no TcdA exotoxin (left), 50 ng/mL of TcdA exotoxin with 1% total volume FD-CF reaction DNA null control (center), and 50 ng/mL TcdA exotoxin with 1% total volume of anti-TcdA-STFL FD-CF reaction (right).

(C) Percentage of Vero cells exhibiting cell-rounding morphology after 24 hr of incubation with TcdA exotoxin and different dilutions of FD-CF reactions in complete media. Experiments were performed in triplicate; data are shown as mean ± SD.

(D) Viability of Vero cells after 48 hr of incubation with TcdA exotoxin and different dilutions of FD-CF reactions. All data were normalized to the no-TcdA toxin, PBS-only control and are shown as mean ± SD, n = 3.

(E) Chart showing receptor-targeted cell therapeutics using FD-CF conjugates of STFL-anti-HER2-DARPin and SC-*P. aeruginosa* exotoxin. Cell viability was monitored for HER2 ± cell lines incubated with different dilutions (v/v) of FD-CF reactions including a DNA null control. All data were normalized to media-only (–) controls and are shown as mean ± SD, n = 3.

(F) Confocal microscopy showing affinity-fluorescent conjugates. $HER2^{+}$ and $HER2^{-}$ cells were probed using FD-CF STFL-anti-HER2 DARPin conjugated to YFP-SC and detected by anti-FLAG, anti-mouse-ATTO655, and YFP fluorescence.

(G) GFP^{+} and GFP^{-} cells were probed using FD-CF anti-GFP-STFL Nanobody and were probed with anti-FLAG and anti-mouse-ATTO655.

Scale bars, 50 microns.

While one of the intended uses of these Ab conjugates, as on-demand, economical lab reagents, may not demand purification, therapeutics administered by injection would require prior purification. Therefore, in addition to the FLAG-based affinity purification option, we explored a simple and particularly inexpensive method based on the cellulose binding module (CBM3) domain from *Clostridium thermocellum*, which has high affinity to cellulose, a cheap and sustainable resource (Wan et al., 2011) (Figure S3B). A CBM3-tagged TcdA Nanobody was expressed from FD-CF reagent and readily isolated from background using regenerated amorphous cellulose (RAC), showing a relative purity of ~95%, which strongly supports this approach for inexpensive purification of on-demand biosynthesis products (Figure S3C).

We next focused on bioactivity tests, beginning with an evaluation of the affinity and specificity of the DARPin and Nanobody conjugates for their cognate targets via an immunolabeling assay. Dot blots were used to test four Nanobody PhoAP-SC conjugates against four antigens. Imaging revealed high specificity for each of the conjugates with very low cross-reactivity (Figure 5A). PhoAP-SC was selected over SanaAP-SC due to a nearly 2-fold higher peak activity (Figure S3D). To demonstrate potential therapeutic applications for FD-CF Ab conjugates, we subjected the anti-TcdA Nanobody to a *C. difficile* exotoxin cell-based assay. TcdA is an exotoxin generated during *C. difficile* infection that causes extensive damage of the intestinal mucosa, promotes inflammatory responses, and can be fatal. An anti-TcdA Nanobody has previously been shown to neutralize the exotoxin (Hussack et al., 2011). Here, Vero cells incubated with exotoxin were completely protected from toxicity (cell-rounding and eventual death) in the presence of FD-CF Nanobody (Figure 5B)

in a dose-dependent manner (Figure 5C), which was also supported by a colorimetric tetrazolium-based cell viability assay (Figure 5D).

Next, we tested the bioactivity of the anti-HER2 DARPin conjugated to exotoxin A domain from *P. aeruginosa*, previously used in immunotoxin therapy (Wolf and Elsässer-Beile, 2009). FD-CF DARPin-toxin was applied to $HER2^-$ cells (HEK293T) and $HER2^+$ breast cancer cells (ATCC HCC1954) in culture at a ratio of 1:500 and 1:1,000. After 3 days, cell viability was assessed, and we found that, at 1:500, the anti-HER2 DARPin-toxin led to a 75% reduction in $HER2^+$ cells compared to $HER2^-$ cells, with selective killing at >50%, using a 1:1,000 dilution (Figure 5E). In contrast, $HER2^-$cells showed little to no signs of toxicity at these dilutions, demonstrating selective targeting.

This DARPin also has great value in clinical diagnostic and research settings. The DARPin and complementary YFP-SpyCatcher were applied to fixed $HER2^+$ and $HER2^-$ cells that were then probed with an anti-FLAG primary Ab and anti-mouse ATTO 655 secondary Ab (Figure 5F). The merged images indicated specific labeling of overlapping regions in only the $HER2^+$ cells. GFP^+ NCI-H1975 cells (BBCTG) and GFP^- HCC-1143 control cells (ATCC) were probed with a FD-CF anti-GFP Nanobody, followed by anti-FLAG probing, as described above, resulting in specific labeling of the GFP^+ cells (Figure 5G). These results establish the potential to manufacture on-demand affinity domains directly conjugated to fluorescent proteins, as well as the ability to integrate in-house-manufactured products with commercially available Abs.

Combinatorial Biosynthesis of Small Molecules

Violacein is a purple chromobacterial pigment with antibacterial, antitrypanosomatid, and anticancer properties and is the result of a five-enzyme transformation of two L-tryptophan molecules occurring in *Chromobacterium violaceum* (Figure 6A and Table S1). In light of previous reports of production in vitro (Balibar and Walsh, 2006; Garamella et al., 2016; Nguyen et al., 2015), we chose to test this pathway's compatibility with the FD-CF format for on-demand therapeutic applications. Particularly, we hypothesized that a combinatorial approach, similar to that applied to the affinity and output domains, could be applied for small-molecule production, as well. To this end, the expression of each enzyme in the metabolic pathway (VioA, B, C, D, E) was first tested using FD-CF reaction pellets and confirmed via WB (Figure 6B). Next, FD-CF reaction pellets were rehydrated with combinations of VioA-E template amounts to establish the optimal concentration for each component's DNA that would lead to the highest levels of violacein, which was identified using MS (Figures S4A and S4B). Although it is impossible to conduct the CF expression at pH 9.25 (the optimal value for violacein enzymes), adjusting the CF reaction pH from 7.6 to 8.0 yielded improved pathway performance (Figures S4C and S4D). Having characterized optimal conditions, MS was used to confirm violacein biosynthesis and showed increased pigment production over time (Figure 6C). Finally, to test the proposition of mixing and matching DNA elements for combinatorial small-molecule synthesis, templates encoding the pathway enzymes were selectively combined and reactions were monitored over time (Figures 6D–6G and S5). Analysis confirmed the production of the five expected compounds from the given gene combinations, as depicted (Figures 6C–6G). Using UHPLC-MS analysis with a commercially available standard, violacein and deoxyviolacein were quantified at 1.0 μM and 4.7 μM, respectively (Figures 6C and 6G).

DISCUSSION

Portable Biomolecule Manufacturing

We have presented a platform for portable biomanufacturing that by complementing centralized production may fill many unmet needs. Indeed, efforts in decentralizing pharmaceutical production summarized in recent reports send a powerful message that there is a clear global need for alternatives to centralized biomanufacturing. In one project (Adamo et al., 2016), researchers sought to alleviate drug storage or offer the means for quick reaction to epidemics by constructing a customized instrument (weighing 100 kg) for the chemistry-based production of pharmaceuticals. Another recent work (Perez-Pinera et al., 2016) described local biomanufacturing using a compact, microfluidic bioreactor housing genetically engineered yeast. While both approaches are impressive, the former requires specialized operational skill and focuses mostly on products that are already shipped as dry tablets. The latter system is accompanied by biosafety regulations surrounding biosynthesis using live, genetically engineered cells and relies on a complex microfluidic device. Both approaches lack the flexibility and ease of operation of the abiotic, FD-CF format presented here, which was employed to produce a diverse range of proteins, including AMPs, vaccines, designer affinity-output domains, and enzymes for small-molecule therapeutics production. Crucially, our functional validations, including a vaccine-elicited immune response and breast cancer cell targeting, strongly support the concept of generating bioactive, protein-based tools and therapies on demand. Furthermore, only the addition of water and incubation at body temperature are required to activate point-of-use biosynthesis. These examples suggest that FD-CF biomanufacturing can be extended to a range of sophisticated applications and is a viable option for the much-needed decentralization of therapeutic production.

Rapid Prototyping, Distribution, and Global Health Applications

The CF format is well suited for rapidly prototyping biomanufacturing protocols. In the absence of a cell wall, expression parameters and the DNA encoding the desired output can be rapidly screened for utility. This flexibility was critical for the optimization of violacein production (Figure S4). Indeed, although FD-CF reaction pellets can be used to produce an array of protein types, testing several conditions for a protein may be required. The straightforward screening nature of a CF format has important implications for the rapid, low-cost development and dissemination of therapeutics in response to health crises.

The conventional distribution of biomolecules is bound to cold-chain requirements and their underlying costs, which severely impact delivery to remote or low-resource regions (Kumru et al., 2014; Wolfson et al., 2008). A central benefit of using FD-CF pellets is the ability to transport the material at room

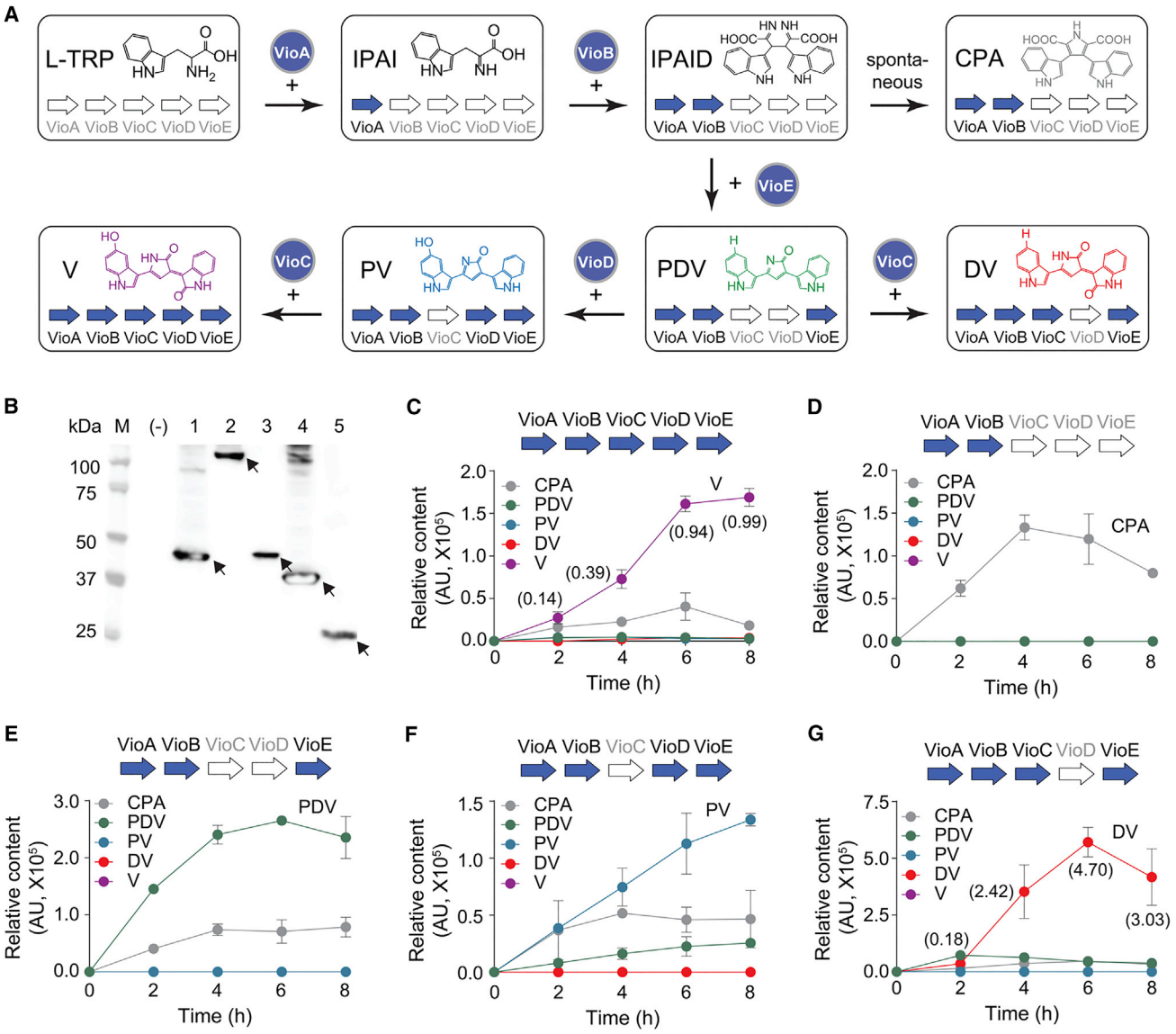

Figure 6. FD-CF Combinatorial Small-Molecule Biosynthesis

(A) Schematic of the biosynthetic violacein pathway. Violacein is produced through five enzymatic steps from two molecules of L-tryptophan. Various combinations of five enzymes yield different small molecules. CPA, chromopyrrolic acid; DV, deoxyviolacein; IPAI, indole-3-pyruvic acid imine; IPAID, IPAI dimer; L-trp, L-tryptophan; PDV, prodeoxyviolacein; PV, proviolacein; V, violacein.

(B) Anti-FLAG WB confirming expression of each enzyme in the violacein pathway.

(C–G) Combinatorial production of small molecules. FD-CF reaction pellets containing the substrate and cofactors were rehydrated with the indicated combinations of template DNA encoding VioA, VioB, VioC, VioD, or VioE. Samples taken from each reaction mixture every 2 hr up to 8 hr were analyzed by UHPLC-MS. Violacein and deoxyviolacein were quantified using a commercially available standard, and numbers in the parentheses of (C) and (G) indicate the measured concentrations in μM. AU, arbitrary units. Data represent the mean ± SD of three replicates.

temperature for local production of therapeutics. The option of keeping the FD-CF reagent and DNA separate until use results in a flexible manufacturing capacity for responding to therapeutic needs as they arise. One may envision deploying either a premixed or separate library of molecular programs, encoding a virtual pharmacy that can be implemented rapidly via hydration. This concept could provide the means for local staple biomanufacturing or annual vaccine distribution or for a response to pathogen outbreaks. For example, using a local, small-batch format, influenza vaccine production could be rapidly re-positioned when vaccine effectiveness is found to be low (CDC, 2016a), an option that is difficult to apply with conventional vaccine production techniques.

The FD-CF format can produce diagnostic tools for clinical labs at low cost. In principle, conjugated anti-HER2 DARPins could be manufactured on site and applied to determine HER2

status as part of treatment decisions for breast cancer. Poor populations are increasingly concentrated in urban areas where portably manufactured diagnostics could be accessible. This is especially important given that the cancer rate in low- and middle-income countries is growing and globally leads to more deaths than malaria, tuberculosis, and HIV/AIDS combined (Lopes et al., 2013). In many cases, the diagnostic products do not require purification, with non-binding material removed via washes. In fact, even in certain therapeutic scenarios, such as the topical administration of AMPs, removal of background proteins would not be required. Also, Nanobodies are resistant to stomach acids and gastrointestinal proteases (Ebrahimizadeh et al., 2013), which highlights the potential for portable biosynthesis of ingestible therapeutics that would not require isolation from expression machinery. However, for affinity-conjugated therapeutics that require purification, one may envision a microfluidic chip-based approach for use in the field, similar to previous efforts (Millet et al., 2015). For further cost reduction, this concept could be merged with cellulose-based purification (Figure S3B). At $0.31 per gram, the RAC matrix is five and seven orders of magnitude less expensive than Ni-NTA and anti-FLAG resins, respectively (Table S2).

Economics of FD-CF Biomanufacturing

A driving motivation for this project is to ultimately provide a platform for low-cost bioproduction. Current CF systems range from 3–68 cents per μL with protein yields of 200–2,300 μg/mL (Caschera and Noireaux, 2014; Hayes, 2012; Kwon and Jewett, 2015). As an example of potential CF manufacturing costs, a recent study reported that an influenza vaccine mixed at point of use with adjuvant provides patient immunization with only 3.75 μg antigen/dose (Mulligan et al., 2014). Assuming a protein yield of 200 μg/mL, this dose could be produced using FD-CF reaction pellets for $0.56–$12.75. The scaled-up production and in vivo validation of the DT vaccine presented here provide an opportunity to calculate specific costs per dose. QFWB indicated the DT5 and DT6 yields using commercial recombinant reagent (NEB; E6800L) at 768 ng/μL and 1341 ng/μL, respectively. With a DT vaccine dosage of 20.8 μg (Schwendeman et al., 1995; WHO, 2014b), this translates to a respective cost per dose of $18.41 and $10.54 ($0.68/μL). Importantly, we demonstrated that FD-CF reactions from in-house lysates yielded DT5 at levels comparable to a commercial, lysate-based system (Promega; L1110) for less than a tenth of the cost ($0.03/μL versus $0.38/μL) (Figure S2E). The CDC cost of a DTaP vaccine (diphtheria, tetanus, pertussis) is $16.73 per dose (CDC, 2016b). Of note, besides the direct cost per dose, the expense of cold-chain distribution can account for 80% of a vaccine's cost (Kols and Sherris, 2000). Also, vaccine wastage in the developing world, which would be reduced by on-demand production, is estimated by the World Health Organization and United Nations Children's Fund to be as high as 50% (Setia et al., 2002).

In another cost breakdown, the semiquantitative yield measured for AMPs produced using the recombinant system (Figure S1C and Table S2) places the manufacturing cost of the highest-producing peptide, Cecropin B, at $3.10–$3.60 per μg, which, while more expensive than commercial sources ($1.88/μg; Sigma C1796-.1MG), represents a price that could be attractive for portable applications or screening assays in research. Additionally, future applications could include the dynamic biosynthesis of AMPs in response to the presence of a detected pathogen by combining a sensory component to a therapeutic output, which would require the AMP to exist in pre-translational, genetic form. We also showed that AMPs can be produced using in-house FD-CF reaction pellets with a yield that out-performed the commercial counterpart (Promega L1110) ($0.03/μL versus $0.38/μL) (Figure S1A). It is also reasonable to expect that technological improvements (Swartz, 2006) will continue to reduce costs. These advances will include disruptive approaches, such as the Nanopatch vaccine technology, which requires 1/100th of the amount of vaccine compared to conventional intramuscular injections (Fernando et al., 2010). Therefore, although current numbers already support reasonable cost, emerging technologies will likely improve the economics for FD-CF biomanufacturing by orders of magnitude.

Portable Molecular Manufacturing of the Future

Looking forward, we envision a system that merges FD-CF diagnostics with biomanufacturing, such as their combination into wound dressings, allowing FD-CF systems to autonomously monitor patients for infection and respond with therapeutic biosynthesis. It is also intriguing to consider a more distant future in which new technology would allow for on-site DNA synthesis. Coupled with FD-CF reaction pellets, this capability would provide users with both the physical genetic program and the manufacturing tools in a form of "molecular 3D printing." Scenarios of extreme conditions, including war zones or space travel, may leave individuals with unanticipated diagnostic or therapeutic needs, whereupon electronic transmission of biosynthesis instructions could be implemented on site. In summary, the FD-CF format provides a new venue for biomanufacturing that promises to stimulate further innovation in synthetic biology and, perhaps ultimately, to have a transformative effect on the distribution of global health.

STAR★METHODS

Detailed methods are provided in the online version of this paper and include the following:

- KEY RESOURCES TABLE
- CONTACT FOR REAGENT AND RESOURCE SHARING
- EXPERIMENTAL MODEL AND SUBJECT DETAILS
  - Mice
  - Mammalian cell culture
  - Bacteria
- METHOD DETAILS
  - General template design and preparation
  - General cell-free reaction preparation and lyophilization protocol
  - In-house cell-free extract preparation
  - Quantitative Fluorescent Western Blot
  - AMP production
  - Portable vaccine production
  - Affinity and output domain production
  - Small molecule synthesis

SUPPLEMENTAL INFORMATION

Supplemental Information includes five figures and two tables and can be found with this article online at http://dx.doi.org/10.1016/j.cell.2016.09.013.

AUTHOR CONTRIBUTIONS

K.P. designed and performed experiments and co-wrote the manuscript. S.S. designed and performed AMP and vaccine experiments and co-wrote the manuscript. P.Q.N. designed and performed affinity-conjugate experiments. J.W.L. designed and performed vaccine and violacein experiments. N.D. designed and performed affinity-conjugate, vaccine and violacein experiments. D.B. designed and performed vaccine experiments. T.F. designed and performed immunofluorescence imaging. F.R.M. designed and built violacein constructs and prepared standard compounds. Y.F. designed and built violacein constructs. A.V. performed animal work for vaccine trial. M.L. performed MS of violacein reaction extracts. C.N.B. designed experiments. N.S.J. designed experiments. J.J.C. designed experiments and co-wrote the manuscript. All authors edited the manuscript.

ACKNOWLEDGMENTS

We thank Chikdu Shivalila and Bryan Hassel from the Wyss Institute for assistance with project logistics, as well as Ning Mao and Dana Braff for experimental guidance. We are grateful to Amanda Graveline, Matthew Pezone and Jeff Way from the Wyss Institute, for guidance and assistance with animal studies. The work was supported by the Wyss Institute for Biologically Inspired Engineering, the Ragon Institute, the Paul G. Allen Frontiers Group, and the Defense Threat Reduction Agency grant HDTRA1-14-1-0006.

Received: June 23, 2016
Revised: August 16, 2016
Accepted: September 6, 2016
Published: September 22, 2016

REFERENCES

Adamo, A., Beingessner, R.L., Behnam, M., Chen, J., Jamison, T.F., Jensen, K.F., Monbaliu, J.-C.M., Myerson, A.S., Revalor, E.M., Snead, D.R., et al. (2016). On-demand continuous-flow production of pharmaceuticals in a compact, reconfigurable system. Science *352*, 61–67.

Amiram, M., Haimovich, A.D., Fan, C., Wang, Y.-S., Aerni, H.-R., Ntai, I., Moonan, D.W., Ma, N.J., Rovner, A.J., Hong, S.H., et al. (2015). Evolution of translation machinery in recoded bacteria enables multi-site incorporation of nonstandard amino acids. Nat. Biotechnol. *33*, 1272–1279.

Balibar, C.J., and Walsh, C.T. (2006). In vitro biosynthesis of violacein from L-tryptophan by the enzymes VioA-E from Chromobacterium violaceum. Biochemistry *45*, 15444–15457.

Botyanszki, Z., Tay, P.K.R., Nguyen, P.Q., Nussbaumer, M.G., and Joshi, N.S. (2015). Engineered catalytic biofilms: Site-specific enzyme immobilization onto E. coli curli nanofibers. Biotechnol. Bioeng. *112*, 2016–2024.

Brito, L.A., and Singh, M. (2011). Acceptable levels of endotoxin in vaccine formulations during preclinical research. J. Pharm. Sci. *100*, 34–37.

Caschera, F., and Noireaux, V. (2014). Synthesis of 2.3 mg/ml of protein with an all Escherichia coli cell-free transcription-translation system. Biochimie *99*, 162–168.

CDC (2016a). Seasonal Influenza Vaccine Effectiveness, 2005-2016; http://www.cdc.gov/flu/professionals/vaccination/effectiveness-studies.htm. Accessed August 2016.

CDC (2016b). CDC Vaccine Price List: http://www.cdc.gov/vaccines/programs/vfc/awardees/vaccine-management/price-list/. Accessed August 2016.

Chubukov, V., Mukhopadhyay, A., Petzold, C.J., Keasling, J.D., and Martín, H.G. (2016). Synthetic and systems biology for microbial production of commodity chemicals. Npj Syst. Biol. Appl. *2*, 16009.

Collier, R.J. (2006). Multi-mutant diphtheria toxin vaccines. US Patent 7115725 B2.

Dandinarasaiah, M., Vikram, B.K., Krishnamurthy, N., Chetan, A.C., and Jain, A. (2013). Diphtheria Re-emergence: Problems Faced by Developing Countries. Indian J Otolaryngol Head Neck Surg *65*, 314–318.

Danino, T., Prindle, A., Kwong, G.A., Skalak, M., Li, H., Allen, K., Hasty, J., and Bhatia, S.N. (2015). Programmable probiotics for detection of cancer in urine. Sci. Transl. Med. *7*, 289ra84.

Desmyter, A., Spinelli, S., Roussel, A., and Cambillau, C. (2015). Camelid nanobodies: killing two birds with one stone. Curr. Opin. Struct. Biol. *32*, 1–8.

Dimitrov, D.S. (2012). Therapeutic proteins. Methods Mol. Biol. *899*, 1–26.

Doshi, R., Chen, B.R., Vibat, C.R.T., Huang, N., Lee, C.-W., and Chang, G. (2014). In vitro nanobody discovery for integral membrane protein targets. Sci. Rep. *4*, 6760.

Dudley, Q.M., Karim, A.S., and Jewett, M.C. (2015). Cell-free metabolic engineering: biomanufacturing beyond the cell. Biotechnol. J. *10*, 69–82.

Ebrahimizadeh, W., Mousavi Gargari, S., Rajabibazl, M., Safaee Ardekani, L., Zare, H., and Bakherad, H. (2013). Isolation and characterization of protective anti-LPS nanobody against V. cholerae O1 recognizing Inaba and Ogawa serotypes. Appl. Microbiol. Biotechnol. *97*, 4457–4466.

Fernando, G.J.P., Chen, X., Prow, T.W., Crichton, M.L., Fairmaid, E.J., Roberts, M.S., Frazer, I.H., Brown, L.E., and Kendall, M.A.F. (2010). Potent immunity to low doses of influenza vaccine by probabilistic guided micro-targeted skin delivery in a mouse model. PLoS ONE *5*, e10266.

Fossati, E., Ekins, A., Narcross, L., Zhu, Y., Falgueyret, J.-P., Beaudoin, G.A.W., Facchini, P.J., and Martin, V.J.J. (2014). Reconstitution of a 10-gene pathway for synthesis of the plant alkaloid dihydrosanguinarine in Saccharomyces cerevisiae. Nat. Commun. *5*, 3283.

Garamella, J., Marshall, R., Rustad, M., and Noireaux, V. (2016). The All E. coli TX-TL Toolbox 2.0: A Platform for Cell-Free Synthetic Biology. ACS Synth. Biol. *5*, 344–355.

Gaspar, D., Veiga, A.S., and Castanho, M.A.R.B. (2013). From antimicrobial to anticancer peptides. A review. Front Microbiol *4*, 294.

Giannini, G., Rappuoli, R., and Ratti, G. (1984). The amino-acid sequence of two non-toxic mutants of diphtheria toxin: CRM45 and CRM197. Nucleic Acids Res. *12*, 4063–4069.

Gibson, D.G., Young, L., Chuang, R.-Y., Venter, J.C., Hutchison, C.A., 3rd, and Smith, H.O. (2009). Enzymatic assembly of DNA molecules up to several hundred kilobases. Nat. Methods *6*, 343–345.

Goerke, A.R., and Swartz, J.R. (2008). Development of cell-free protein synthesis platforms for disulfide bonded proteins. Biotechnol. Bioeng. *99*, 351–367.

Green, A.A., Silver, P.A., Collins, J.J., and Yin, P. (2014). Toehold switches: de-novo-designed regulators of gene expression. Cell *159*, 925–939.

Gupta, R.K., Collier, R.J., Rappuoli, R., and Siber, G.R. (1997). Differences in the immunogenicity of native and formalinized cross reacting material (CRM197) of diphtheria toxin in mice and guinea pigs and their implications on the development and control of diphtheria vaccine based on CRMs. Vaccine *15*, 1341–1343.

Hayes, C. (2012). Biomolecular Breadboards:Protocols:cost estimate. http://www.openwetware.org/wiki/Biomolecular_Breadboards:Protocols:cost_estimate. Accessed August 2016.

Hussack, G., Arbabi-Ghahroudi, M., van Faassen, H., Songer, J.G., Ng, K.K.-S., MacKenzie, R., and Tanha, J. (2011). Neutralization of Clostridium difficile toxin A with single-domain antibodies targeting the cell receptor binding domain. J. Biol. Chem. *286*, 8961–8976.

Karim, A.S., and Jewett, M.C. (2016). A cell-free framework for rapid biosynthetic pathway prototyping and enzyme discovery. Metab. Eng. *36*, 116–126.

Kobayashi, H., Kaern, M., Araki, M., Chung, K., Gardner, T.S., Cantor, C.R., and Collins, J.J. (2004). Programmable cells: interfacing natural and engineered gene networks. Proc. Natl. Acad. Sci. USA *101*, 8414–8419.

Kols, A., and Sherris, J. (2000). HPV vaccines: promise and challenges http://www.path.org/files/jsrp13710.pdf. Accessed August 2016.

Kontermann, R.E. (2012). Dual targeting strategies with bispecific antibodies. MAbs *4*, 182–197.

Kumru, O.S., Joshi, S.B., Smith, D.E., Middaugh, C.R., Prusik, T., and Volkin, D.B. (2014). Vaccine instability in the cold chain: mechanisms, analysis and formulation strategies. Biologicals *42*, 237–259.

Kwon, Y.-C., and Jewett, M.C. (2015). High-throughput preparation methods of crude extract for robust cell-free protein synthesis. Sci. Rep. *5*, 8663.

Lee, K.-H., Kwon, Y.-C., Yoo, S.J., and Kim, D.-M. (2010). Ribosomal synthesis and in situ isolation of peptide molecules in a cell-free translation system. Protein Expr. Purif. *71*, 16–20.

Lehar, S.M., Pillow, T., Xu, M., Staben, L., Kajihara, K.K., Vandlen, R., DePalatis, L., Raab, H., Hazenbos, W.L., Morisaki, J.H., et al. (2015). Novel antibody-antibiotic conjugate eliminates intracellular S. aureus. Nature *527*, 323–328.

Lopes, G. de L., Jr., de Souza, J.A., and Barrios, C. (2013). Access to cancer medications in low- and middle-income countries. Nat. Rev. Clin. Oncol. *10*, 314–322.

Martemyanov, K.A., Shirokov, V.A., Kurnasov, O.V., Gudkov, A.T., and Spirin, A.S. (2001). Cell-free production of biologically active polypeptides: application to the synthesis of antibacterial peptide cecropin. Protein Expr. Purif. *21*, 456–461.

Millet, L.J., Lucheon, J.D., Standaert, R.F., Retterer, S.T., and Doktycz, M.J. (2015). Modular microfluidics for point-of-care protein purifications. Lab Chip *15*, 1799–1811.

Mulligan, M.J., Bernstein, D.I., Frey, S., Winokur, P., Rouphael, N., Dickey, M., Edupuganti, S., Spearman, P., Anderson, E., Graham, I., et al. (2014). Point-of-Use Mixing of Influenza H5N1 Vaccine and MF59 Adjuvant for Pandemic Vaccination Preparedness: Antibody Responses and Safety. A Phase 1 Clinical Trial. Open Forum Infect. Dis. *1*, ofu102.

Ng, C.T., Jaworski, J.P., Jayaraman, P., Sutton, W.F., Delio, P., Kuller, L., Anderson, D., Landucci, G., Richardson, B.A., Burton, D.R., et al. (2010). Passive neutralizing antibody controls SHIV viremia and enhances B cell responses in infant macaques. Nat. Med. *16*, 1117–1119.

Nguyen, P.Q., Botyanszki, Z., Tay, P.K.R., and Joshi, N.S. (2014). Programmable biofilm-based materials from engineered curli nanofibres. Nat. Commun. *5*, 4945.

Nguyen, P.H.B., Wu, Y., Guo, S., and Murray, R.M. (2015). Design Space Exploration of the Violacein Pathway in Escherichia coli Based Transcription Translation Cell-Free System (TX-TL). bioRxiv.

Noireaux, V., and Libchaber, A. (2004). A vesicle bioreactor as a step toward an artificial cell assembly. Proc. Natl. Acad. Sci. USA *101*, 17669–17674.

Palmenberg, A.C. (1982). In vitro synthesis and assembly of picornaviral capsid intermediate structures. J. Virol. *44*, 900–906.

Pardee, K., Green, A.A., Ferrante, T., Cameron, D.E., DaleyKeyser, A., Yin, P., and Collins, J.J. (2014). Paper-based synthetic gene networks. Cell *159*, 940–954.

Pardee, K., Green, A.A., Takahashi, M.K., Braff, D., Lambert, G., Lee, J.W., Ferrante, T., Ma, D., Donghia, N., Fan, M., et al. (2016). Rapid, Low-Cost Detection of Zika Virus Using Programmable Biomolecular Components. Cell *165*, 1255–1266.

Patel, K.G., Ng, P.P., Levy, S., Levy, R., and Swartz, J.R. (2011). Escherichia coli-based production of a tumor idiotype antibody fragment–tetanus toxin fragment C fusion protein vaccine for B cell lymphoma. Protein Expr. Purif. *75*, 15–20.

Perez-Pinera, P., Han, N., Cleto, S., Cao, J., Purcell, O., Shah, K.A., Lee, K., Ram, R., and Lu, T.K. (2016). Synthetic biology and microbioreactor platforms for programmable production of biologics at the point-of-care. Nat. Commun. *7*, 12211.

Plückthun, A. (2015). Designed ankyrin repeat proteins (DARPins): binding proteins for research, diagnostics, and therapy. Annu. Rev. Pharmacol. Toxicol. *55*, 489–511.

Ryabova, L.A., Desplancq, D., Spirin, A.S., and Plückthun, A. (1997). Functional antibody production using cell-free translation: effects of protein disulfide isomerase and chaperones. Nat. Biotechnol. *15*, 79–84.

Salehi, A.S.M., Smith, M.T., Bennett, A.M., Williams, J.B., Pitt, W.G., and Bundy, B.C. (2016). Cell-free protein synthesis of a cytotoxic cancer therapeutic: Onconase production and a just-add-water cell-free system. Biotechnol. J. *11*, 274–281.

Sánchez, C., Braña, A.F., Méndez, C., and Salas, J.A. (2006). Reevaluation of the violacein biosynthetic pathway and its relationship to indolocarbazole biosynthesis. ChemBioChem *7*, 1231–1240.

Schwendeman, S.P., Costantino, H.R., Gupta, R.K., Siber, G.R., Klibanov, A.M., and Langer, R. (1995). Stabilization of tetanus and diphtheria toxoids against moisture-induced aggregation. Proc. Natl. Acad. Sci. USA *92*, 11234–11238.

Scott, A.M., Wolchok, J.D., and Old, L.J. (2012). Antibody therapy of cancer. Nat. Rev. Cancer *12*, 278–287.

Setia, S., Mainzer, H., Washington, M.L., Coil, G., Snyder, R., and Weniger, B.G. (2002). Frequency and causes of vaccine wastage. Vaccine *20*, 1148–1156.

Smith, M.T., Berkheimer, S.D., Werner, C.J., and Bundy, B.C. (2014). Lyophilized Escherichia coli-based cell-free systems for robust, high-density, long-term storage. Biotechniques *56*, 186–193.

Spirin, A.S., Baranov, V.I., Ryabova, L.A., Ovodov, S.Y., and Alakhov, Y.B. (1988). A continuous cell-free translation system capable of producing polypeptides in high yield. Science *242*, 1162–1164.

Sullivan, C.J., Pendleton, E.D., Sasmor, H.H., Hicks, W.L., Farnum, J.B., Muto, M., Amendt, E.M., Schoborg, J.A., Martin, R.W., Clark, L.G., et al. (2016). A cell-free expression and purification process for rapid production of protein biologics. Biotechnol. J. *11*, 238–248.

Sun, Z.Z., Hayes, C.A., Shin, J., Caschera, F., Murray, R.M., and Noireaux, V. (2013). Protocols for implementing an Escherichia coli based TX-TL cell-free expression system for synthetic biology. J. Vis. Exp. *79*, e50762.

Swartz, J. (2006). Developing cell-free biology for industrial applications. J. Ind. Microbiol. Biotechnol. *33*, 476–485.

Torella, J.P., Gagliardi, C.J., Chen, J.S., Bediako, D.K., Colón, B., Way, J.C., Silver, P.A., and Nocera, D.G. (2015). Efficient solar-to-fuels production from a hybrid microbial-water-splitting catalyst system. Proc. Natl. Acad. Sci. USA *112*, 2337–2342.

Wan, W., Wang, D., Gao, X., and Hong, J. (2011). Expression of family 3 cellulose-binding module (CBM3) as an affinity tag for recombinant proteins in yeast. Appl. Microbiol. Biotechnol. *91*, 789–798.

Wang, R.E., Liu, T., Wang, Y., Cao, Y., Du, J., Luo, X., Deshmukh, V., Kim, C.H., Lawson, B.R., Tremblay, M.S., et al. (2015). An immunosuppressive antibody-drug conjugate. J. Am. Chem. Soc. *137*, 3229–3232.

Welsh, J.P., Lu, Y., He, X.-S., Greenberg, H.B., and Swartz, J.R. (2012). Cell-free production of trimeric influenza hemagglutinin head domain proteins as vaccine antigens. Biotechnol. Bioeng. *109*, 2962–2969.

WHO (2014a). Temperature Sensitivity of Vaccines; http://www.who.int/immunization/programmes_systems/supply_chain/resources/VaccineStability_EN.pdf. Accessed August 2016.

WHO (2014b). World Health Organization: Information sheet observed rate of vaccine reactions Diphtheria, pertussis, tetanus vaccines. http://www.who.int/vaccine_safety/initiative/tools/DTP_vaccine_rates_information_sheet.pdf. Accessed August 2016.

Wolf, P., and Elsässer-Beile, U. (2009). Pseudomonas exotoxin A: from virulence factor to anti-cancer agent. Int. J. Med. Microbiol. *299*, 161–176.

Wolfson, L.J., Gasse, F., Lee-Martin, S.-P., Lydon, P., Magan, A., Tibouti, A., Johns, B., Hutubessy, R., Salama, P., and Okwo-Bele, J.-M. (2008). Estimating the costs of achieving the WHO-UNICEF Global Immunization Vision and Strategy, 2006-2015. Bull. World Health Organ. *86*, 27–39.

Zakeri, B., Fierer, J.O., Celik, E., Chittock, E.C., Schwarz-Linek, U., Moy, V.T., and Howarth, M. (2012). Peptide tag forming a rapid covalent bond to a protein, through engineering a bacterial adhesin. Proc. Natl. Acad. Sci. USA *109*, E690–E697.

Zawada, J.F., Yin, G., Steiner, A.R., Yang, J., Naresh, A., Roy, S.M., Gold, D.S., Heinsohn, H.G., and Murray, C.J. (2011). Microscale to manufacturing scale-up of cell-free cytokine production–a new approach for shortening protein production development timelines. Biotechnol. Bioeng. *108*, 1570–1578.

Zhang, Y.-H.P., Cui, J., Lynd, L.R., and Kuang, L.R. (2006). A transition from cellulose swelling to cellulose dissolution by o-phosphoric acid: evidence from enzymatic hydrolysis and supramolecular structure. Biomacromolecules *7*, 644–648.

Zichel, R., Mimran, A., Keren, A., Barnea, A., Steinberger-Levy, I., Marcus, D., Turgeman, A., and Reuveny, S. (2010). Efficacy of a potential trivalent vaccine based on Hc fragments of botulinum toxins A, B, and E produced in a cell-free expression system. Clin. Vaccine Immunol. *17*, 784–792.

STAR★METHODS

KEY RESOURCES TABLE

REAGENT or RESOURCE	SOURCE	IDENTIFIER
Antibodies		
Mouse monoclonal anti-FLAG-HRP conjugate	Abcam	Cat#ab49763; RRID: AB_869428
Mouse monoclonal anti-FLAG M2 antibody	Sigma-Aldrich	Cat#F1804; RRID: AB_262044
Goat polyclonal anti-mouse IgG atto 655	Sigma-Aldrich	Cat#50283; RRID: AB_1137655
Mouse anti-FLAG-DyLight650 conjugated fluorescent antibody	Abcam	Cat#ab117492; RRID: AB_10903191
Rabbit His-tag Antibody, pAb	GenScript	Cat#A00174-40; RRID: AB_914703
Mouse monoclonal anti-FLAG M2 antibody	Sigma-Aldrich	Cat#F3165; RRID: AB_259529
Goat Anti-Mouse IgG (H + L)-HRP Conjugate	Bio-Rad	Cat#1721011; RRID: AB_11125936
Goat Anti-Rabbit IgG (H + L)-HRP Conjugate	Bio-Rad	Cat#1706515; RRID: AB_11125142
Chemicals, Peptides, and Recombinant Proteins		
Imject Alum Adjuvant	Thermo Scientific	77161
Anti-DYKDDDDK G1 Affinity Resin	GeneScript	L00432
3X FLAG peptide	Sigma-Aldrich	F4799
Flavin adenine dinucleotide (FAD)	Sigma-Aldrich	F6625-25MG
Hemin	Sigma-Aldrich	H9039-1G
Dimethyl sulfoxide (DMSO)	Alfa Aesar	42780
Nicotinamide adenine dinucleotide, reduced form (NADH)	Sigma-Aldrich	N8129-50MG
L-Tryptophan	Sigma-Aldrich	T8941-25G
Ammonium iron(III) sulfate	Sigma-Aldrich	34249-1L
5-aminolevulinic acid hydrochloride	Sigma-Aldrich	A7793-500MG
Violacein and deoxyviolacein	Sigma-Aldrich	V9389-1MG
Protector RNase Inhibitor	Roche	03335399001
RNase Inhibitor, Murine	New England Biolabs	M0314L
Disulfide bond enhancer	New England Biolabs	N6820S
Microcrystalline cellulose powder	Sigma-Aldrich	435236
Phosphoric acid	Sigma-Aldrich	W290017
Sodium carbonate	Sigma-Aldrich	230952
Recombinant GFP	Clontech	632373
Recombinant HIV-p24-gag	ProSpec	HIV-123
Inactivated rotavirus viral lysate	Microbix Biosystems	EL-35-03
Clostridium difficile exotoxin TcdA	List Laboratories	152C
Factor Xa protease	New England Biolabs	P8010S
Xarrest agarose	EMD Millipore	69038-3
Antifoam 204	Sigma-Aldrich	A8311-50ML
Custom-synthesized AMPs	Lifetein	
Critical Commercial Assays/Kits		
LAL Chromogenic Endotoxin Quantitation Kit	Thermo Scientific	88282
BCA Protein Assay Kit	Thermo Scientific	23227
PURExpress	New England Biolabs	E6800L
S30 T7 High-Yield Protein Expression	Promega	L1110
Mouse Anti-Diphtheria Toxin IgG ELISA kit	Alpha Diagnostics International	940-120-DMG
Diphtheria Toxoid/Toxin ELISA kit	Alpha Diagnostics International	940-DTX-AG1
CDP-STAR AP substrate	Sigma-Aldrich	C0712
MTS CellTiter 96 AQueous One Solution Cell Proliferation Assay	Promega	G3580

(*Continued on next page*)

Continued

REAGENT or RESOURCE	SOURCE	IDENTIFIER
Deposited Data		
Plasmid pET15b-vioA DNA sequence file	NCBI GenBank	GenBank: KX461959
Plasmid pET15b-vioB DNA sequence file	NCBI GenBank	GenBank: KX461960
Plasmid pET15b-vioC DNA sequence file	NCBI GenBank	GenBank: KX461961
Plasmid pET15b-vioD DNA sequence file	NCBI GenBank	GenBank: KX461962
Plasmid pET21-vioE DNA sequence file	NCBI GenBank	GenBank: KX461963
Experimental Models: Cell Lines		
Grivet: Vero cells	ATCC	CCL-81
Human: Mammary gland HCC-1954	ATCC	CRL-2328
Human: Mammary gland HCC-1143	ATCC	CRL-2321
Human: Embryonic Kidney HEK293T	In-house lab cell line	
Human: GFP-labeled NCI-H1975 cells	Genecopoeia	SL003
Experimental Models: Organisms/Strains		
E. coli: Rosetta 2(DE3) cells	EMD Millipore	71400
E. coli: Mach1 competent cells	Thermo Scientific	C862003
E. coli: Turbo competent cells	New England Biolabs	C2984H
E. coli: MG1655 cells	In-house lab strain	
B. subtilis: JH642	In-house lab strain	
Mouse: FVB/NCrl	Charles River	207
Recombinant DNA		
Diptheria antigen: pET22b DT 51E/148K	Addgene	11081
Anthrax antigen: pET22b-PA WT	Addgene	11079
Violacein pathway: BBa_J72214-BBa_J72090	Addgene	40782
For remaining sequences please see Table S1		
Sequence-Based Reagents		
Please See Table S1		
Software and Algorithms		
Prism 6	Graphpad	Version 6.0e
MyCurveFit (4 parameter logistic regression model for standard curves)	MyAssays Ltd	www.mycurvefit.com

CONTACT FOR REAGENT AND RESOURCE SHARING

For further information and request of reagents please contact the corresponding author Jim Collins (jimjc@mit.edu).

EXPERIMENTAL MODEL AND SUBJECT DETAILS

Mice

All mice used in the study were the FVB/NCrl strain obtained from Charles River Laboratories (#207; Wilmington, MA). Mice were housed and maintained on standard diet (LabDiet; 5058) in an AAALAC-accredited facility under controlled temperature, humidity, and light (12:12-h light:dark cycle) with continuous access to food and water. Animal experiments were performed in accordance with guidelines of the Institutional Animal Care and Use Committee of Harvard Medical School (Protocol 04998).

Mammalian cell culture

Mammalian cells were cultured as monolayers at 37°C with 5% CO_2 in a humidified incubator. All media were supplemented with 10% fetal bovine serum (FBS) and for each cell type, were applied as follows: HCC-1954 (overexpressing HER2; ATCC; CRL-2338) and HCC-1143 (under-expressing HER2; ATCC; CRL-2321) breast cancer cells were cultured in RPMI 1640 medium. HEK293T and GFP-labeled NCI-H1975 cells (Genecopoeia; SL003) were cultured in DMEM. Vero cells (ATCC; CCL-81) were grown in Eagle's Minimal Essential Medium supplemented with 100 U/mL of penicillin and 100 μg/mL of streptomycin.

Bacteria

Liquid bacterial cultures were grown in Luria broth (LB) at 37°C in shaking incubators. *E. coli* Rosetta™2(DE3) (EMD Millipore) were used to prepare in-house, cell-free lysates. *E. coli* Mach1 (ThermoFisher; C862003) and *E. coli* Turbo (New England Biolabs (NEB); C2984H) were used for template cloning. *E. coli* MG1655 and *B. subtilis* JH642 were used for AMP growth inhibition assays.

METHOD DETAILS

General template design and preparation

DNA sequences encoding manufacturing targets were derived from Addgene constructs or from literature, codon optimized for *E. coli* and synthesized as gBlocks or oligos by Integrated DNA Technologies (IDT). All sequences are described in Supplemental Information (Table S1). Cloning and plasmid propagation were performed using either Mach1 (ThermoFisher; C862003) or Turbo (New England Biolabs (NEB; C2984H) competent *E. coli* cells. For AMPs, gBlocks or oligos encoding peptides were amplified by polymerase chain reaction (PCR) using primers designed according to the PURExpress guidelines (NEB; E6800L) to yield linear expression templates or cloned into a T7-expression plasmid (Table S1). For vaccine manufacturing, templates were cloned into a T7-expression plasmid system using Gibson assembly (Gibson et al., 2009). The Botulinum toxin E gene (Zichel et al., 2010) was cloned into a T7- vector forming pET15b-HcE. pET22b DT 51E/148K (Addgene plasmid #11081) was used as a backbone to construct DT1-6. pET22b-PA WT (Addgene plasmid # 11079) was used as a construct for anthrax antigen production. Nanobody and DARPin sequences were cloned into pET15b. The His-YFP-SpyCatcher and α-Amylase-SpyCatcher plasmids have been previously cloned and described (Botyanszki et al., 2015; Nguyen et al., 2014). The PhoAP, SanaAP, PAexotoxin, and CDexotoxin output domains were DNA synthesized and subcloned into pDEST14-His-YFP-SpyCatcher plasmid, replacing the YFP domain. DNA constructs for enzymes of the violacein pathway [*vioA*, *vioB*, and *vioC* from Addgene plasmid #40782; *vioD* synthesized based on the sequence provided in Registry of Standard Biological Parts (BBa_K274002); *vioE* from pVio1-2 (Sánchez et al., 2006)] were cloned into T7 vector to yield pET15b-vioA, -vioB, -vioC, and -vioD, and pET21-vioE (GenBank: KX461959, KX461960, KX461961, KX461962, KX461963).

General cell-free reaction preparation and lyophilization protocol

CF reactions using commercial systems PURExpress (NEB) or S30 T7 High-Yield Protein Expression (Promega; L1110)) were prepared on ice and supplemented with Protector RNase Inhibitor (Roche; 03335399001) or RNase Inhibitor, Murine (NEB; M0314L). Reactions were flash-frozen in liquid nitrogen and lyophilized overnight to obtain FD pellets. Template DNA was added prior to lyophilization or during rehydration, which activated and restored samples to original volumes, described below. AMPs were produced by rehydrating PURExpress pellets with purified PCR-based template at 10 ng/μL and incubated for two hours at 37°C. AMPs were also produced using either the S30 T7 system (Promega) or in-house lysate by rehydrating pellets with plasmid template at 15 ng/μL, and incubated in a Thermomixer at 1,200 RPM for two hours at 37°C. Vaccine antigens were similarly prepared using 15, 30, 45, or 60 ng/μL input plasmid. Affinity and output pellets used 10 ng/μL input plasmid. For small-molecule production, FD-CF pellets were prepared using the S30 T7 system (Promega) supplemented with the following components: Protector RNase inhibitor (0.5% v/v), flavin adenine dinucleotide (5 μM), hemin (17 μM, stock solution prepared in DMSO), nicotinamide adenine dinucleotide, reduced form (200 μM), nicotinamide adenine dinucleotide phosphate, reduced form (100 μM), L-tryptophan (2 mM), ammonium iron sulfate (100 μM), and 5-aminolevulinic acid (40 μM). To adjust pH, 0.2, 0.5, 0.8, and 1.2 μl of NaOH (1 M) per 10 μl reaction were supplemented to make pH 8.0, pH 8.5, pH 9.0, and pH 9.5, respectively. Plasmid templates were added during pellet rehydration, then incubated at 30°C for 8 hr.

In-house cell-free extract preparation

E. coli Rosetta™2(DE3) (EMD Millipore) were grown in 400 ml of LB containing chloramphenicol (34 μg/mL) and 0.1 mM IPTG at 37°C at 250 rpm. Cells were harvested in mid-exponential growth phase (OD_{600} ~0.6), and cell pellets were washed three times with ice cold Buffer A containing 10 mM Tris-Acetate pH 8.2, 14 mM magnesium acetate, 60 mM potassium glutamate, and 2 mM DTT, and were flash frozen and stored at −80°C. Cell extract was prepared as described in the previous publication (Kwon and Jewett, 2015). Briefly, cell pellets were thawed and resuspended in 1 ml of Buffer A per 1 g of wet cells and sonicated in an ice-water bath. Total sonication energy to lyse cells was determined by using the sonication energy equation for BL21 Star™ (DE3), [Energy] = [Volume (μL)] – 33.6] · 1.8^{-1}. A Q125 Sonicator (Qsonica) with 3.174 mm diameter probe at a frequency of 20 kHz was used for sonication. A 50% amplitude in 10 s on/off intervals was applied until the required input energy was met. Lysate was then centrifuged at 12,000 rcf for 10 min at 4°C, and the supernatant was incubated at 37°C at 300 rpm for 1 hr. The supernatant was centrifuged again at 12,000 rcf for 10 min at 4°C, and was flash frozen and stored at −80°C until use. Using a previously published cell-free reaction protocol (Sun et al., 2013), reaction mixtures were composed of 26.6% (v/v) of in-house lysate, 1.5 mM each amino acid except leucine (1.25 mM), 1 mM DTT, 50 mM HEPES (pH 8.0), 1.5 mM ATP and GTP, 0.9 mM CTP and UTP, 0.2 mg/mL tRNA, 0.26 mM CoA, 0.33 mM NAD, 0.75 mM cAMP, 0.068 mM folinic acid, 1 mM spermidine, 30 mM 3-PGA, 2% PEG-8000, 1 mM IPTG

and 0.5% (v/v) Protector RNase Inhibitor. Optimal potassium glutamate (20-140mM) and magnesium glutamate (3-15mM) concentrations were determined for each target product. Reactions were flash-frozen in liquid nitrogen and lyophilized overnight to obtain freeze-dried pellets.

Quantitative Fluorescent Western Blot

FD-CF reaction samples (using PURExpress (NEB)) were prepared. Samples were centrifuged and the supernatant containing only soluble protein was collected for quantification. These, and dilutions of FLAG-tagged protein standard (Sigma-Aldrich; P7457), were loaded onto NuPAGE gels, electrophoresed in MES buffer, and transferred onto PVDF membranes. The membrane was air-dried overnight, rehydrated in methanol, washed in water, and transferred to PBS. Blocking of the membrane was performed in 4% Blotto milk solids (Rockland; B501-0500) + 2% cold water fish gelatin (Sigma-Aldrich; G7041) in PBS for 1 hr. Probing was performed in the dark using PBS + 0.1% Tween-20 and 0.02% SDS and an anti-FLAG-DyLight650 conjugated fluorescent antibody (Abcam; ab117492) at a 1:1000 dilution for 1.5 hr. Extensive washes in PBS + 0.1% Tween-20 were followed by PBS only. The fluorescent immunoblots were imaged on a Fluorchem M instrument using the near infra-red setting. Each fluorescent Western blot was analyzed independently to control for differences in background and integration times. Signal intensity was determined for the appropriate bands using the Image Studio Lite software (LICOR).

AMP production

Protein electrophoresis, staining, and blotting

AMP samples were boiled for 3 min in 2x Tricine sample buffer (Bio-Rad; 161-0739), loaded in 16.5% polyacrylamide Tris/Tricine precast gels (Bio-Rad, Mini-PROTEAN, 4563065), and run at 200 mA for 4.5 hr. For Coomassie staining, gels were fixed for one hour in 12% trichloroacetic acid and one hour in 40% EtOH, 10% acetic acid, followed by 14 hr staining in QC Colloidal Coomassie (Bio-Rad; 161-0803), 2 hr de-staining in water, and finally imaged using a Gel Logic system (Carestream Mol. Imaging). For Western blots, proteins were transferred to 0.2 μm nitrocellulose membrane (Bio-Rad; 1620112) for 90 min at 90 V using a wet transfer system (Bio-Rad; 1703930), and hybridized overnight at 4°C with either α-His (GenScript; A00174-40) or α-Flag-M2 (Sigma-Aldrich; F3165) primary Ab's in 3% milk-TBST, then with secondary HRP-conjugated Ab's (Bio-Rad; #1721011 and #1706515) at room temperature for one hour, and finally imaged using the Gel Logic system.

Peptide cleavage and filtration

AMP versions containing FLAG affinity tags and Factor Xa cleavage sites were produced as described above, purified using Anti-DYKDDDDK G1 Affinity Resin (GenScript; L00432), and eluted with a DYKDDDDK competitor peptide (GenScript; RP10586-1), according to the manufacturer's instructions. Purified protein (and alternatively, crude protein) was cleaved overnight using Factor Xa protease (NEB; P8010S) and Factor Xa protease was removed using Xarrest agarose (EMD Millipore; 69038-3), according to the manufacturers' instructions. Non-tagged AMPs were isolated via molecular weight cut off filtration (MWCO) by adjusting samples to 350 mM NaCl (to dissociate peptides from ribosomal machinery) followed by centrifugation through a 10K Microcon column (EMD Millipore; MRCPRT010) and collection of flow-through.

Semi-quantification analysis

Semi-quantification analysis of crude and MWCO AMP preparates was performed using peptide standards from a commercial source (LifeTein). For each of the four tested AMPs, crude reactions, retentant (> 10 kDa), and flow-through (< 10 kDa) fractions originating from 4 μl cell-free reactions were subjected to SDS-PAGE and Coomassie staining alongside a loaded gradient of identical commercial peptides ranging from 125 ng to 1000 ng for gel intensity approximation.

Growth inhibition assays for AMPs

E. coli MG1655 or *B. subtilis* JH642 were grown overnight at 37°C in LB, diluted 1:100, grown to OD_{600} 0.5, diluted to 10^4 cells/mL in LB containing 0.005% Antifoam 204 (Sigma-Aldrich; A8311-50ML) to eliminate micro-bubbles, and distributed into wells of a 96-well plate containing 10 μl of the finished AMP cell-free transcription and translation reaction, Null reaction, or water. All wells were overlaid with 10 μl mineral oil to prevent evaporation and condensation. OD_{600} was recorded every 30 min for 18 hr at 37°C using a SpectraMax M3 plate-reader.

Portable vaccine production

For each construct, 2 μl of sample were run on denaturing 10%–20% Novex™ WedgeWell Tris-Glycine Mini Gels (Invitrogen) and stained with Coomassie Brilliant Blue G-250 (Bio-Rad). To test binding of DT5 and DT6 to anti-DT toxin/toxoid Ab, an ELISA kit specific for DT (Alpha Diagnostic International; 940-DTX-AG1) was used. Equal dilutions of each CF reaction were processed according to manufacturer's instructions. To produce DT5 vaccine for an animal test, 0.9 ml of FD-CF NEB reaction mixture was prepared. For a "mock injection" negative control, a DNA Null sample was likewise prepared in which the DNA template encoding the DT5 gene was omitted from the cell-free reaction. FLAG-tag purification was performed using Anti-DYKDDDDK G1 Affinity Resin (GenScript; L00432), and eluted with a 3X FLAG peptide (Sigma; F4799). For subsequent animal injection, eluents of purified DT5 antigen and the DNA Null control were exchanged to PBS using a 10 kDa Microcon column (EMD Millipore; MRCPRT010), and concentrated to 100 μg/mL. An LAL assay (Thermo Scientific; 88282) was used to check endotoxin levels.

Animal model methods

The DT5 antigen and negative control were mixed 1:1 with a vaccine adjuvant (Imject Alum; Thermo Scientific) and were incubated at room temperature with shaking for 30 min. Five- to six-week-old female mice in group of five were immunized with the DT5 or negative control, and 4 female mice with the same age were used as a habitat (no injection) control. Each mouse was injected subcutaneously with 2.5 μg of DT5 or the negative control on day 0, day 7 and day 14. Serum samples were obtained on day 0 (before injection), day 21, day 28 and day 42, and were stored at −20°C. Animal experiments were performed in accordance with guidelines of the Institutional Animal Care and Use Committee of Harvard Medical School (Protocol 04998).

Analysis of immune response in mouse model

Serum samples were collected from vaccinated mice, negative control mice that were injected with the DNA Null mock sample, and habitat control (non-injected) mice, on days 0 (before injection), 21, 28 and 42, and were stored at −20°C. To analyze the immune response by DT5 antigen, an ELISA kit specific for anti-diphtheria IgG (Alpha Diagnostic International, Catalog No. 940-120-DMG) was used. A four-parameter logistic regression model was used to obtain the standard curve, and anti-diphtheria IgG levels (U/mL) were determined by interpolation.

Affinity and output domain production

Covalent conjugation reactions

Affinity-SpyTag-FLAG-tag and Output-SpyCatcher products were mixed at a 1:1 or 1:2 volumetric ratio to a final 5 μl in HEPES buffered saline (50 mM HEPES, pH 7.5 and 150 mM NaCl) and incubated for 2 hr at 37°C for isopeptide bond formation.

Immunodetection of products

For Western blots, 1 μl of cell-free reactions was loaded onto SDS-PAGE 4%–15% NuPAGE gels (ThermoFisher) using MES running buffer followed by transfer to nitrocellulose membranes using the iBlot 2 apparatus (ThermoFisher). The membranes were air-dried for 2 hr and probed using the SNAP i.d. vacuum-assisted protein detected system (Millipore). Membranes were blocked with TBST + 5% BSA and then probed with a 1:1000 dilution of anti-FLAG-HRP antibody (Abcam; ab49763) in TBST for 10 min, washed, developed with SuperSignal West Pico Chemiluminescent substrate (ThermoFisher; 34080) for 5 min, and imaged in a FluorChem M (Protein Simple). Dot blot detection against natively structured antigen was performed using recombinant GFP (Clontech; 632373), recombinant HIV-p24-gag (ProSpec; HIV-123), inactivated rotavirus viral lysate (Microbix Biosystems; EL-35-03), and purified *Clostridium difficile* exotoxin TcdA (List Laboratories; 152C). All dot blots were performed using Dot-Blot Microfiltration Apparatus (Bio-Rad), according to manufacturer's instructions. Briefly, each antigen was diluted with TBST to 50 ng/μL, and 50 μl was added to the apparatus and allowed to drain by gravity for 1 hr, followed by blocking with TBST + 2% BSA for 30 min and washing. Probing was performed with 1:250 TBST-diluted freeze-dried, cell-free produced anti-HIV, anti-GFP, anti-Rotavirus, and anti-TcdA reactions conjugated to PhoAP-SC. After washing, blots were incubated in CDP-STAR AP substrate (Sigma; C0712) for 10 min, and imaged with a FluorChem M.

CBM3-based purification

The RAC was prepared as previously described (Zhang et al., 2006) using microcrystalline cellulose (Sigma; 435236) and the final slurry resuspended to a final concentration of 10 mg/mL. FD-CF CBM3-anti-TcdA-STFL Nanobody (65 μL) was added to a 3x volume of RAC slurry (195 μL), incubated at room temperature with gentle shaking for 15 min, and bulk-purified by quickly pelleting the RAC using a table-top minicentrifuge at 5,000 rpm for 1 min and removal of the supernatant. Four 300 μl washes were performed using 50 mM Tris, pH 7.4, 200 mM NaCl, and 10% glycerol. All samples and the final RAC pellet with bound purified protein were directly analyzed by SDS-PAGE Coomassie gels.

In vitro cytotoxicity

The effect of STFL-anti-HER2 DARPin conjugated to PAexotoxin-SC on cell viability was assessed using the MTS test (Promega; CellTiter 96 AQueous One Solution Cell Proliferation Assay). HEK293T and HCC-1954 cells were seeded in a 96-well plate at a density of 5×10^3 cells/well and incubated for 24 hr. Cell-free reaction products of either DARPin-PAexotoxin fusion (1:1 affinity:output template one-pot reaction) or no-DNA template reaction were buffer-exchanged to complete growth media using a 30K Amicon centrifugal filter (EMD Millipore, UFC5030). The media were replaced with 100 μl growth media supplemented with a 1:500 or 1:1000 dilution of buffer-exchanged, FD-CF reaction products of either DARPin-PAexotoxin fusion or no-DNA control, followed by incubation for 72h. Next, complete MTS reagent was added to cells in a 1:5 ratio, followed by incubation for 2 hr. Absorbance was measured at 490 nm on a SpectraMax M5 plate reader. All data were collected from experiments performed in triplicate and measurements were normalized for each cell line to media-only controls. Cell viability was calculated as a ratio of the optical density of treated to untreated cells.

Cell-rounding assay

Vero cells (ATCC; CCL-81) were grown at 37°C, 5% CO_2 in Eagle's Minimal Essential Medium supplemented with 10% FBS, 100 U/mL of penicillin and 100 μg/mL of streptomycin. Confluent cells were seeded onto 96-well plates at a seeding density of $\sim 2 \times 10^4$ cells per well, and grown for one day. TcdA toxin (List Laboratories; 152C) at a total concentration of 50 ng/mL and ten-fold serial dilutions of the unpurified FD-CF expressed anti-TcdA Nanobodies (10 μl volume added) were pre-incubated in complete media at a final volume of 100 μl at 37°C, 5% CO_2 for 15 min, and then added to the Vero cells. After 24 hr, the cells were imaged by phase contrast using a Zeiss Axio Observer Z1 microscope. Random 200 × 200 micron areas of the cells were visually analyzed to obtain cell-rounding counts. After 48 hr, cell viability was assessed as described above using the MTS test.

Immunofluorescence

HCC-1143 and HCC-1954 cells were cultured on glass bottom dishes (Mattek) overnight at 37°C in 5% CO_2. Cells were fixed in 4% paraformaldehyde + 4% sucrose solution in DPBS at room temperature for 15 min, permeabilized in 0.25% Triton X-100 in DPBS at room temp for 10 min, and blocked with DPBS + 10% BSA at 37°C for 30 min. Cells were incubated first with FD-CF affinity reaction products of conjugated STFL-anti-HER2 DARPin:YFP-SC diluted 1:2 in DPBS + 3% BSA, followed by incubation with mouse monoclonal anti-FLAG M2 antibody (Sigma; F1804) at 1:1000, and finally anti-mouse IgG ATTO-655 (Sigma; 50283) at 1:1250 dilution. Cells were counterstained with 100 ng/mL DAPI (ThermoFisher; D1306) for 10 min, washed, and sealed using ProLong Diamond Antifade mounting medium (Life Technologies) and 12 mm circular cover glass (VWR; 89015-724). A similar procedure was used for imaging GFP in NCI-H1975 cells, with HCC-1143 cells as a GFP-negative control, except that FD-CF expressed anti-GFP-STFL Nanobody was used instead. Stained and mounted specimens were imaged on a Leica SP5 X MP Inverted Laser Scanning Confocal Microscope. Confocal Z-stacks were converted to 2-D images using maximum intensity projection by ImageJ, and all images were normalized to the same intensity range values.

Small molecule synthesis

Liquid extraction

Ethyl acetate was used to extract violacein and its precursors from cell-free reactions. Five parts of ethyl acetate were added to each part of reaction samples, and vortexed for 5 min. After allowing phase separation for 5 min, the mixture was frozen in a dry ice/ethanol bath and the ethyl acetate phase was collected and subjected to mass spectrometer analyses.

Quantification and identification

Violacein and its precursor molecules in ethyl acetate extracts were quantified on an Agilent 1290/6140 Ultra High Performance Liquid Chromatography/Mass Spectrometer (UHPLC-ESI-MS) consisting of a 1290 Infinity LC binary pump interfaced with an Agilent 1290 Diode Array Detector, Agilent 1290 Infinity Autosampler, Agilent Thermostat Column Compartment, and Agilent 6140 Quadrupole MSD system. Reverse phase chromatographic resolution was performed using an Agilent ZORBAX RRHD SB-C18 column (2.1 × 100 mm, 1.8 μm) along with 0.1% formic acid in Milli-Q water (solution A) and 0.1% formic acid in acetonitrile (solution B) as mobile phases. Elution was started at 5% solution B and held for 2 min, followed by a linear gradient to 98% solution B over 15 min. Solution B was then held for 2 min at 98% followed by a return to 5% solution B over 1 min for a final 2 min hold. Total run time was 20 min with a flow rate of 0.5 mL/minute. Mass analysis was performed in both ESI ± polarity modes using the following parameters: Nebulizer pressure = 40 psi, dry gas flow = 10 L/minute, dry gas temperature = 300°C, capillary voltage = 2500 V (in + mode) and 2000 V (in – mode). For quantification by MS, the $[M-H]^-$ ions for violacein, proviolacein, deoxyviolacein, and prodeoxyviolacein, along with the $[M+H]^+$ ion for chromopyrrolic acid, were monitored using Selected Ion Monitoring Mode at *m/z* 342, 326, 326, 310, and 386, respectively. Each of the four ion channels had a Dwell time 209 (msec) with an inter-channel delay period of 0.05 s and a polarity switch delay of 0.02 s. Commercially available a violacein (~85%) and deoxyviolacein (~13%) mixture (Sigma-Aldrich; V9389-1MG) was used to calculate violacein and deoxyviolacein yield. An Agilent 1290 HPLC coupled to a Bruker Impact II q-TOF was used for product identification. The same LC column and conditions described above were applied to resolve product molecules. The MS was operated in negative ion mode using the following parameters: Nebulizer pressure = 55 psi, dry gas flow = 12 L/minute, dry gas temperature = 220°C, capillary voltage = 4000 V. Each run was calibrated for *m/z* values using sodium formate clusters with a better than 1 ppm fit. With this method, the mass accuracy is expected to be 5 ppm or better.

QUANTIFICATION AND STATISTICAL ANALYSIS

Statistical analysis

Statistical parameters including the definitions and exact values of n, distributions and deviations are reported in the Figures and corresponding Figure Legends. For bacterial growth inhibition assays, each data point represents the average OD_{600} measured at 30 min intervals for three biological replicates, and error bars represent SD.

For vaccine, affinity-conjugate and violacein calculations, Graph Pad Prism was used to calculate and plot mean ± SD values from replicates (n = 3, otherwise indicated).

Quantification

AMP yield from FD-CF recombinant materials was semiquantitatively approximated via gel band intensity comparison between 4 μl of loaded test samples and commercial peptide standards, loaded in 125 ng increments from 125 to 1000 ng. Two adjacent peptide standard lanes, whose range of band intensity encompassed the band intensity observed in the tested sample's lane, were averaged, and this average was divided by 4 (μL) resulting in an approximation of AMP ng per μL in the loaded test sample.

For small-molecule quantification, using a commercially available violacein (~85%) and deoxyviolacein (~13%) mixture (Sigma-Aldrich; V9389-1MG) as a standard, a four-parameter logistic regression model was used to obtain the standard curve. Violacein and deoxyviolacein levels produced from FD-CF reactions were determined by interpolation.

For Quantitative Fluorescent Western Blots, the bands of interest for each blot were quantified by Image Studio Lite and normalized to the highest intensity band for that blot. The relative intensity of diluted FLAG-BAP protein standard bands were plotted as molar

values and a standard linear curve was calculated. The relative intensity of the experimental protein samples were interpolated using this standard curve to calculate their molar concentrations and then converted to mass values from the predicted molecular weights. The total yield of each freeze-dried cell free reaction was determined using this calculated protein mass per total volume of each reaction loaded on the gel. Values are given as the mean of triplicate blots with standard deviation.

DATA AND SOFTWARE AVAILABLITY

Data Resources

Raw data files of the DNA constructs for the enzymes of the violacein pathway have been deposited with NCBI GenBank as accession numbers GenBank: KX461959, KX461960, KX461961, KX461962, KX461963.

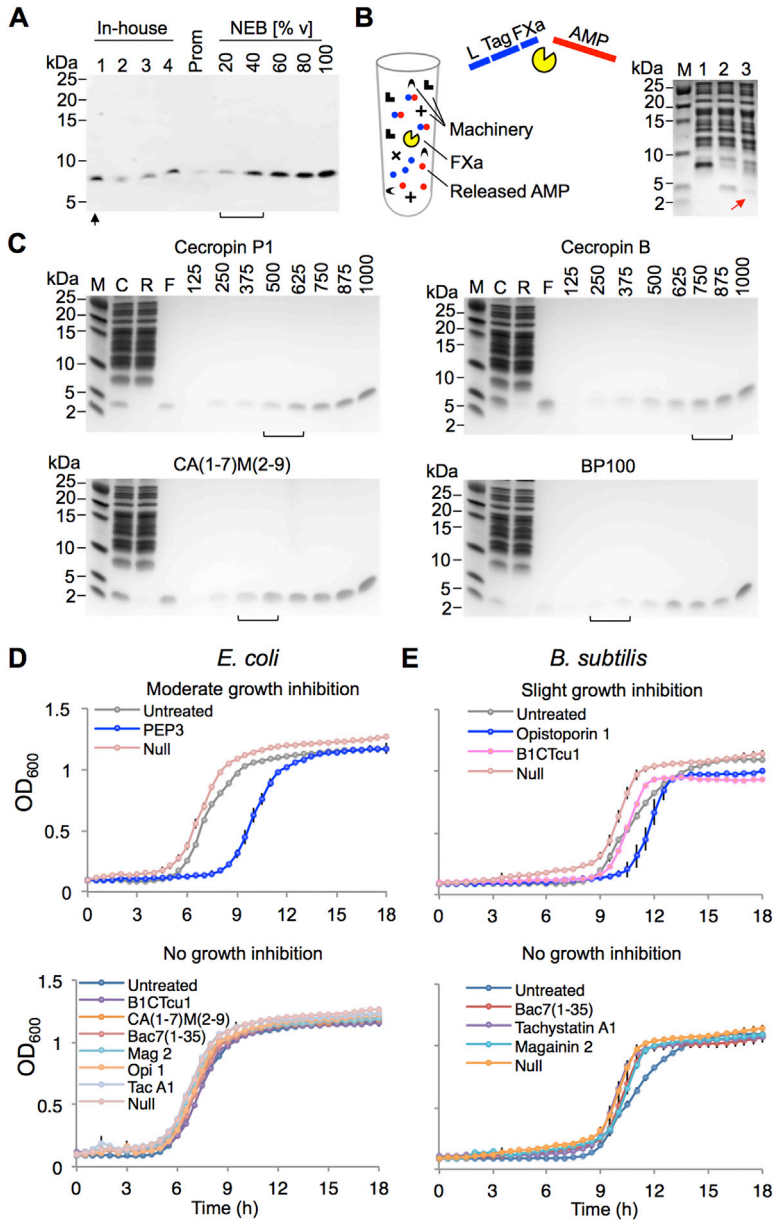

Figure S1. Cell-free Production of AMPs from Freeze-Dried Reactions, Related to Figure 2

(A) Anti-FLAG Western blot comparing expression of tagged Cecropin P1 using In-house lysate (four Mg-Glu + K-Glu concentrations) to an S30 T7 kit (Promega) and a recombinant T7 kit (NEB). Mg-Glu + K-Glu concentrations for lanes 1-4 are 6 + 50, 6 +110, 12 + 110, and 12 + 50 mM, respectively. Equal volumes (10 μL) were loaded for In-house and Promega and semiquantitatively compared to 2, 4, 6, 8, and 10 μL NEB samples. A bracket approximates the band intensity in lane one as comparable to 20%–40% the yield of the NEB system.

(B) At left, schematic describing Factor Xa cleavage of tagged AMP in a crude reaction containing transciption and translation machinery. L; Leader, Tag; His_{x6}- or FLAG-tag, FXa; cleavage site. At right, Coomassie gel; Factor Xa cleavage of FLAG-tagged Cecropin P1 applied to crude product. Lane 1: size control of non-cleaved peptide; lane 2: size control of non-tagged Cecropin P1; lane 3: cleavage reaction. Red arrow points to released AMP.

(C) Coomassie gel; Semiquantitative yield analysis of 4 μL AMP cell-free synthesis fractions from crude (C), MWCO > 10 kDa retentant (R), and MWCO < 10 kDa flow-through (F) samples compared to commercial peptide standards ranging from 125 ng to 1000 ng loaded amounts, as indicated. A bracket indicates the region of band intensity simliar to that seen for the crude and isolated AMPs, resulting in the following approximations: Cecropin P1, 125-156 ng/μL; Cecropin B, 188-219 ng/μL; CA(1-7)M(2-9), 94-125 ng/μL; BP100, 63-94 ng/μL.

(D) Growth inhibition charts. Top: *E. coli* growth moderately inhibited by PEP3 AMP. Bottom: *E. coli* growth uninhibited by the six indicated AMPs.

(E) Growth inhibition charts. Top: *B. subtilis* growth slightly inhibited by the two indicated AMPs. Bottom: *B. subtilis* growth uninhibited by the three indicated AMPs. For (A) and (B), OD_{600} was measured every 30 min for 18 hr. All data points represent the mean from three biological replicates and error bars represent standard deviation.

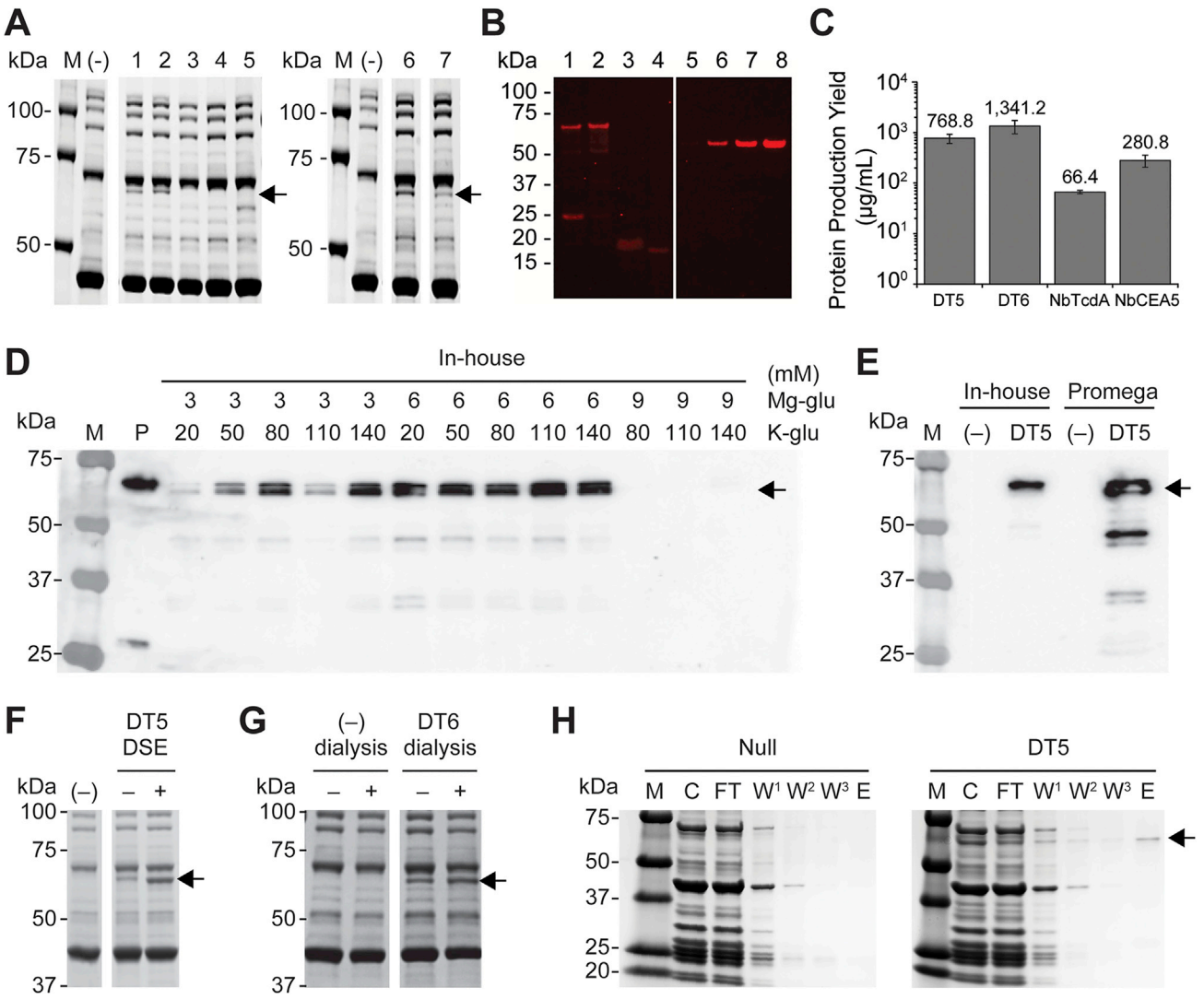

Figure S2. DT Vaccine Expression, Quantification, and Purification, Related to Figures 3 and 4

(A) Coomassie gel showing the expression of five DT vaccine variants (lanes 1-7: DT, DT1, DT2, DT3, DT4, DT5 and DT6). Arrows indicate the expected gel migration for the DT vaccine variants.

(B) Determination of freeze-dried cell free production by Quantitative Fluorescent Western Blots (QFWB). A representative QFWB of is shown, with various freeze-dried cell free reactions (lanes 1-4: 0.5 µl DT5, 0.5 µl DT6, 2 µl anti-TcdA Nanobody, and 0.2 µl anti-CEA5 Nanobody) and FLAG-tagged control protein standards (lanes 5-8: 125, 250, 500, and 1000 ng). All samples and standards were separated, transferred, and probed on the same gel and membrane.

(C) Average protein production yields for three independent freeze-dried cell free reactions for each of the products. Error bars are shown as standard deviation.

(D) Anti-FLAG Western blot showing DT5 expression with different combinations of Mg-glutamate and K-glutamate concentrations. The highest expression was obtained with 6 mM Mg-glutamate and 110 mM K-glutamate). M indicates a molecular weight marker and P indicates a DT5 positive size control produced using a commercial, lysate-based expression system (Promega T7 S30).

(E) Anti-FLAG Western blot comparing expression of DT5 using freeze-dried In-house lysate (at 6 mM Mg-glutamate and 110 mM K-glutamate) to expression using a Promega T7 S30 system. Equal starting material was used and samples of equal volume were loaded. (–) indicates a negative control lacking DNA.

(F) Coomassie gel showing the expression of DT5 with and without DSE. Addition of DSE enhanced the DT5 expression substantially. (–) indicates a negative control lacking DNA.

(G) Coomassie gel showing expression of DT6 with and without dialysis. A 50 µl NEB PURExpress reaction was dialyzed during incubation against 250 µl of NEB PURExpress Buffer A using a 10 kDa cut-off dialysis membrane. (–) indicates a negative control lacking DNA.

(H) Coomassie gels showing FLAG affinity purification of DT5 vaccine (right gel) and null reaction lacking DNA (left gel). Freeze-dried, cell-free starting material (900 µL) was used to prepared vaccine for the full course of the mouse injections. Abbreviations are: M, molecular weight marker; C, crude reaction; FT, flow-through; W1-3, washes; E, elution.

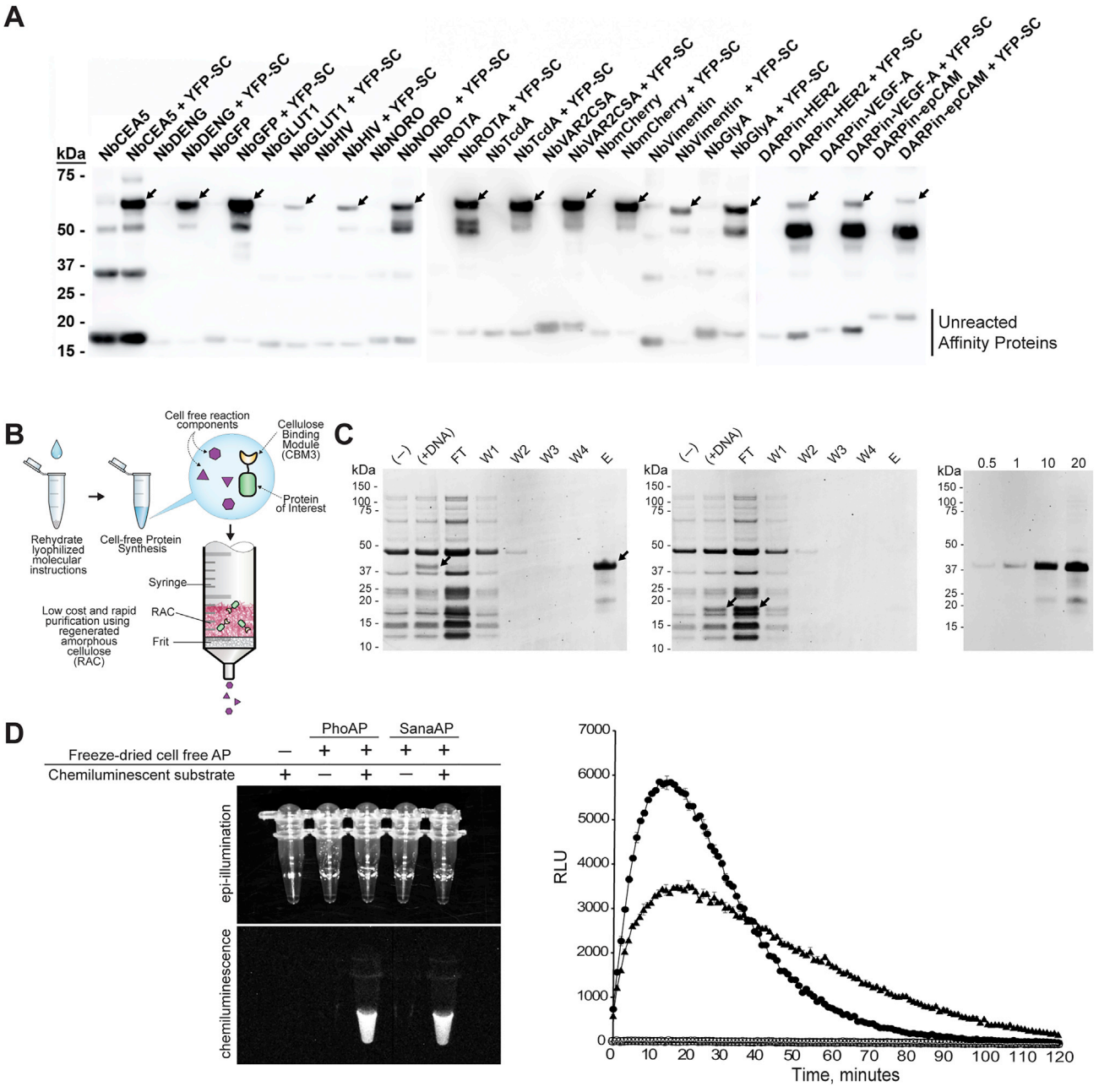

Figure S3. Freeze-Dried, Cell-free Reactions for the Production of On-Demand Affinity Reagents, Related to Figures 4 and 5

(A) Anti-FLAG Western blot showing all freeze-dried, cell-free expressed affinity components containing a SpyTag moiety can successfully react with the SpyCatcher, shown here fused to YFP, to form an intermolecular covalent isopeptide bond.

(B) Low-cost purification scheme of freeze-dried cell free reactions by a Cellulose Binding Module (CBM3) fused to a protein of interest, and regenerated amorphous cellulose (RAC) as the matrix.

(C) Coomassie gels showing purification fractions of freeze-dried expressed CBM3-α-TcdA-STFL Nanobody (indicated by arrows) using RAC (left). Anti-TcdA-STFL Nanobody (indicated by arrows) negative control processed using the same protocol (center). Abbreviations are: FT, flow-through; W1-4, washes; E, elution. Different volumes (μL indicated) of the purified CBM3-anti-TcdA-STFL Nanobody to assess relative purity (right).

(D) PhoAP-SpyCatcher and SanaAP-SpyCatcher output proteins expressed in freeze-dried, cell-free reactions have enzymatically active AP domains, as shown by catalytic processing of a chemiluminescent AP substrate. Direct chemiluminescent imaging is shown (left) as well as a microtiter assay (right) shown as mean ± SE, n = 3. Legend for plot: (□) no enzyme +substrate; (●) PhoAP +substrate, (○) PhoAP -substrate, (▲) SanaAP +substrate, (Δ) SanaAP –substrate.

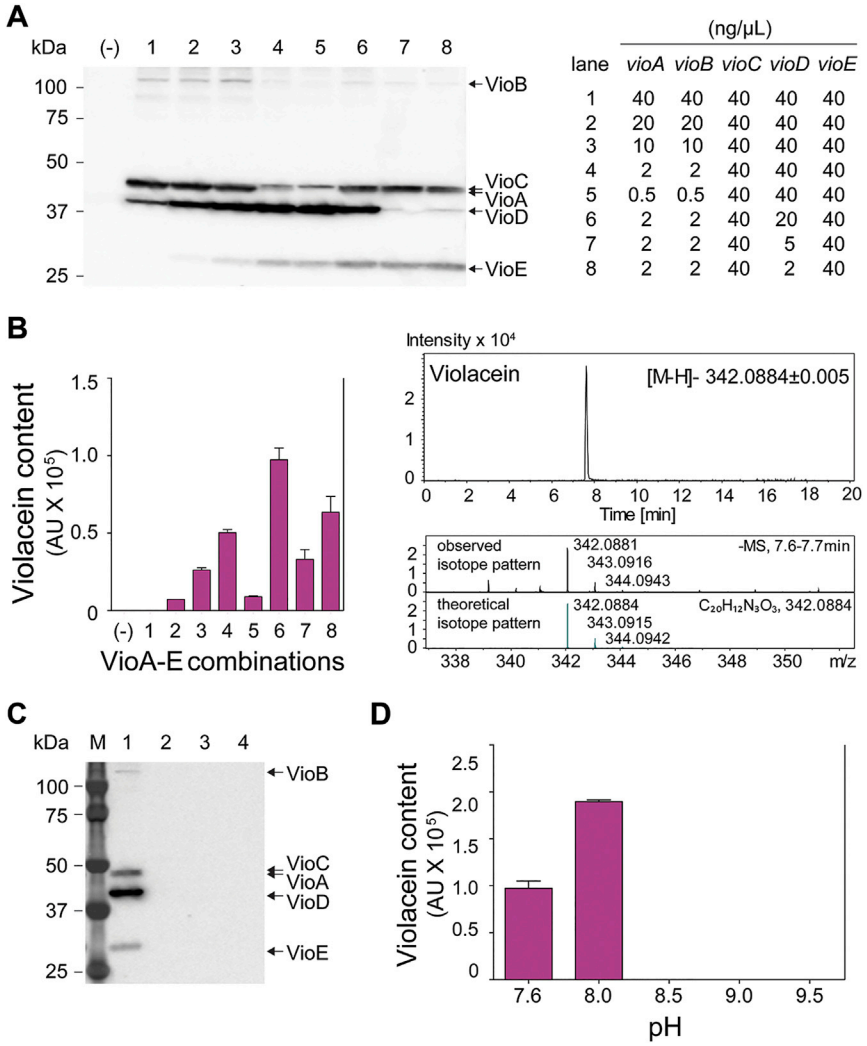

Figure S4. Combination of VioA-E Components and pH Effect for Violacein Biosynthesis Optimization, Related to Figure 6

(A) At left, an anti-FLAG Western blot showing the results of the combined gene ratios (encoding pathway enzymes), with each lane numbered according to the table. At right, a table showing the combination of DNA encoding the VioA-E enzymes at varying concentrations.

(B) Violacein production from different combinations of VioA-E as listed in panel (A). Production of violacein was quantified by UHPLC-MS. VioA-E combination '6' yielded the highest violacein production. Data represent the mean ± SD of three replicates. Violacein was identified by high resolution MS. Right panels show extracted ion chromatogram using chemical formula for violacein with a ± 0.005 Da window in ESI (-) polarity. The observed mass spectral isotopic distribution [M-H]-, acquired from averaging MS scans, fits theoretical data with a mass error of 1.5 ppm or less.

(C) An anti-FLAG Western blot showing expression of the violacein pathway enzymes at different pH levels. Lanes 1-4: pH 8.0, pH 8.5, pH 9.0, and pH 9.5. The standard pH of the rehydrated cell-free solution is 7.6, shown in lane 6 of panel (A).

(D) Quantification of violacein production at different pH levels using UHPLC-MS. Data represent the mean ± SD of three replicates.

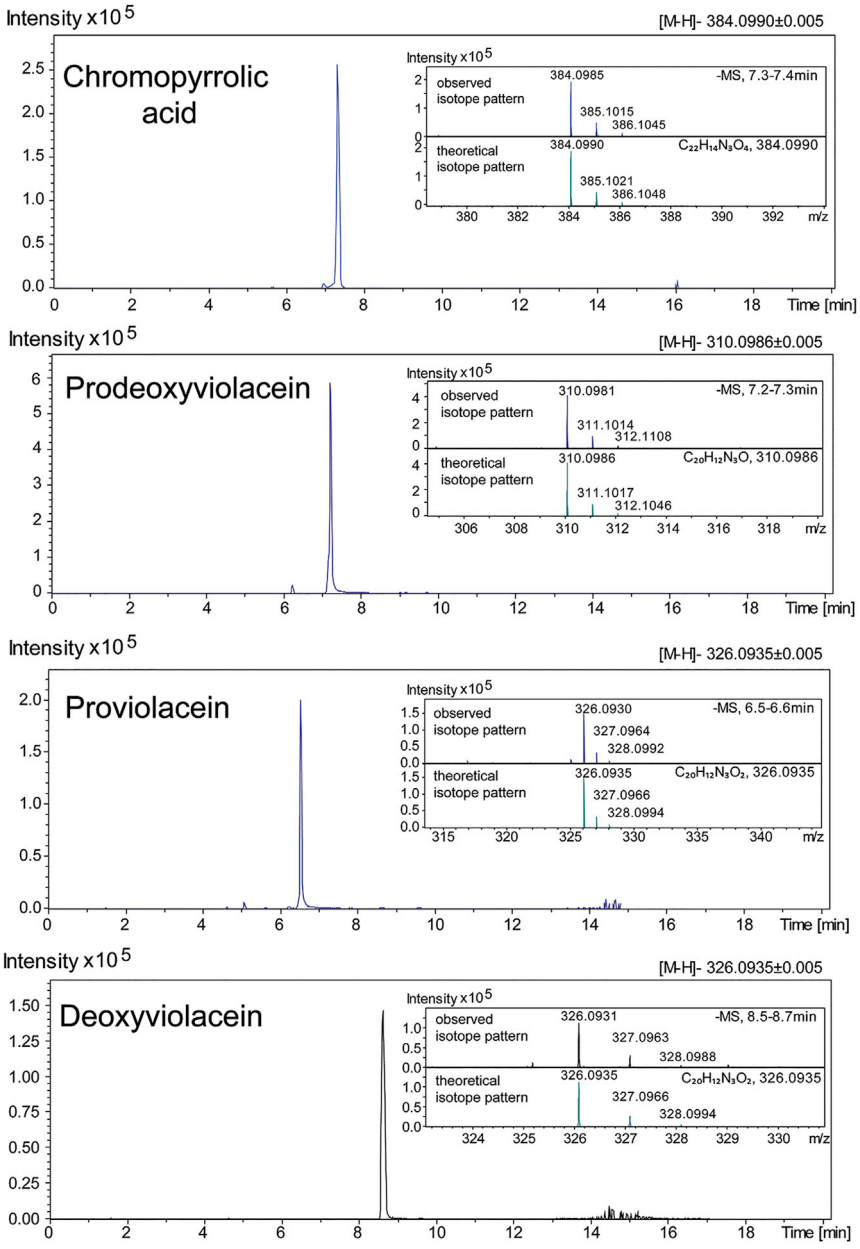

Figure S5. Identification of Products Using High-Resolution MS, Related to Figure 6

Each panel shows extracted ion chromatogram using each chemical formula for chromopyrrolic acid, prodeoxyviolacein, proviolacein, and deoxyviolacein with a ± 0.005Da window in ESI (-) polarity. The observed mass spectral isotopic distribution [M-H]-, acquired from averaging MS scans, fits theoretical data with a mass error of 1.5ppm or less.